LNAPL Distribution and Recovery Model (LDRM)

Volume 1: Distribution and Recovery of Petroleum Hydrocarbon Liquids in Porous Media

Regulatory and Scientific Affairs Department

API PUBLICATION 4760
JANUARY 2007

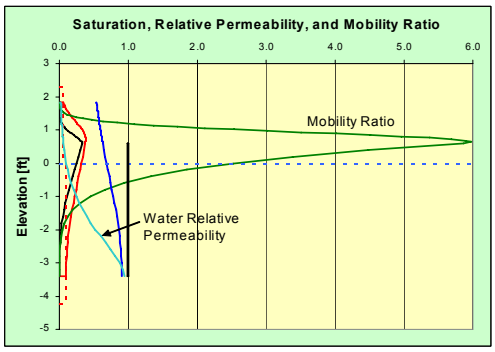

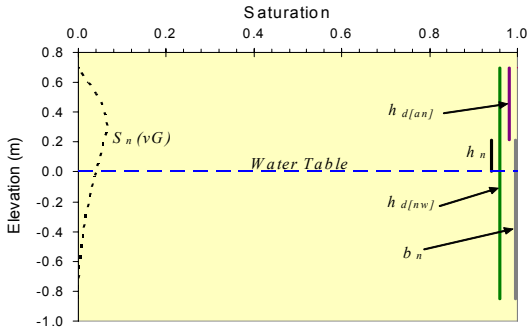

LNAPL Distribution and Recovery Model (LDRM)

Volume 1: Distribution and Recovery of Petroleum Hydrocarbon Liquids in Porous Media

Regulatory and Scientific Affairs Department

API PUBLICATION 4760
JANUARY 2007

Prepared by:

Randall Charbeneau, Ph.D., P.E.
The University of Texas at Austin
Austin, Texas

SPECIAL NOTES

API publications necessarily address problems of a general nature. With respect to particular circumstances, local, state, and federal laws and regulations should be reviewed.

Neither API nor any of API's employees, subcontractors, consultants, committees, or other assignees make any warranty or representation, either express or implied, with respect to the accuracy, completeness, or usefulness of the information contained herein, or assume any liability or responsibility for any use, or the results of such use, of any information or process disclosed in this publication. Neither API nor any of API's employees, subcontractors, consultants, or other assignees represent that use of this publication would not infringe upon privately owned rights.

API publications may be used by anyone desiring to do so. Every effort has been made by the Institute to assure the accuracy and reliability of the data contained in them; however, the Institute makes no representation, warranty, or guarantee in connection with this publication and hereby expressly disclaims any liability or responsibility for loss or damage resulting from its use or for the violation of any authorities having jurisdiction with which this publication may conflict.

API publications are published to facilitate the broad availability of proven, sound engineering and operating practices. These publications are not intended to obviate the need for applying sound engineering judgment regarding when and where these publications should be utilized. The formulation and publication of API publications is not intended in any way to inhibit anyone from using any other practices.

Any manufacturer marking equipment or materials in conformance with the marking requirements of an API standard is solely responsible for complying with all the applicable requirements of that standard. API does not represent, warrant, or guarantee that such products do in fact conform to the applicable API standard.

FOREWORD

Nothing contained in any API publication is to be construed as granting any right, by implication or otherwise, for the manufacture, sale, or use of any method, apparatus, or product covered by letters patent. Neither should anything contained in the publication be construed as insuring anyone against liability for infringement of letters patent.

Suggested revisions are invited and should be submitted to the Director of Regulatory and Scientific Affairs, API, 1220 L Street, NW, Washington, D.C. 20005.

PREFACE

This manuscript (Volume 1) provides background information supporting formulation of the American Petroleum Institute LNAPL Distribution and Recovery Model (LDRM), and is presented as a supplement to API Publication Number 4682, *Free-Product Recovery of Petroleum Hydrocarbon Liquids*, which was published in June 1999, and to API Publication Number 4729, *Models for Design of Free-Product Recovery Systems for Petroleum Hydrocarbon Liquids; A User's Guide and Model Documentation*, which was published in August 2003 and included in the API Interactive LNAPL Guide, Version 2.0. Model scenarios are described for free-product hydrocarbon liquid recovery using single- and dual-pump well systems, skimmer wells, vacuum-enhanced well systems, and trenches. Information on LNAPL distribution in porous media and possible LNAPL movement is discussed, and the basic modeling equations are provided. Use of the LDRM software to compute LNAPL recovery rates, volumes and times is discussed, and example applications are provided in a companion document (Volume 2), which also documents model testing and evaluation. The API LDRM software can be downloaded from API's website at: groundwater.api.org/lnapl.

TABLE OF CONTENTS

LIST OF FIGURES

LIST OF SYMBOLS

A_c	area extent of region of capture for well or trench
A_j	performance coefficient in LNAPL recovery models
b	aquifer thickness
b_a	screened interval for air flow above the water table
b_n	monitoring well LNAPL thickness
b_{nW}	LNAPL thickness in well, constrained by fine-grain-zone
b_w	depth beneath the water table of groundwater flow to a well or trench
d	mean grain-size diameter
D_n	LNAPL specific volume
f_{ar}	mass flux of air in radial direction
f_{az}	mass flux of air in vertical direction
f_r	residual LNAPL f-factor (fraction of initial LNAPL saturation)
f_{rs}	residual LNAPL f-factor (saturated zone)
f_{rv}	residual LNAPL f-factor (vadose zone)
g	gravitational constant
h	fluid head
h_c	capillary pressure head
h_d	displacement pressure head (air-water)
$h_{d[an]}$	air-LNAPL displacement pressure head
$h_{d[nw]}$	LNAPL-water displacement pressure head
$h_{[an]}$	air-LNAPL capillary pressure head (equivalent water head)
$h_{[nw]}$	LNAPL-water capillary pressure head (equivalent water head)
J_a	air-phase hydraulic gradient
J_n	LNAPL hydraulic gradient
J_w	water hydraulic gradient
J_{wz}	vertical water hydraulic gradient (positive upward)
k	intrinsic permeability
K_n	LNAPL hydraulic conductivity
K_{ns}	LNAPL saturated hydraulic conductivity
k_{ra}	air relative permeability
k_{rn}	LNAPL relative permeability
K_{ws}	water saturated hydraulic conductivity
k_{rw}	water relative permeability
$\hat{k}$	upward unit vector
L_T	length of LNAPL recovery trench
M	van Genuchten *M* parameter
$m_{r[nw]}$	LNAPL-water mobility ratio $(= k_{rn}/(k_{rw}\mu_r))$
$\dot{m}_{ar}$	mass rate of flow of air in radial direction
n	porosity
N	van Genuchten *N* parameter
p	fluid pressure
p_a	air pressure
p_c	capillary pressure

$p_{c[an]}$	air-LNAPL capillary pressure
$p_{c[nw]}$	LNAPL-water capillary pressure
p_n	LNAPL pressure
p_{nC}	LNAPL pressure at radius of capture (R_C)
p_{nW}	LNAPL pressure at radius of well (R_W)
p_w	water pressure
p_{wI}	water pressure at radius of influence (R_I)
p_{wW}	water pressure at radius of well (R_W)
$p(r_c)$	fraction of pores of size r_c
q_n	LNAPL volume flux (Darcy velocity)
Q_n	LNAPL discharge
q_{nz}	LNAPL vertical volume flux (positive upward)
q_w	water volume flux (Darcy velocity)
Q_w	water discharge
R_c	radius of capture
R_n	LNAPL recoverable volume
$\bar{r}$	mean radius of curvature of interface between fluid phases
S_e	effective (reduced) saturation
$S_{e[t]}$	effective total liquid saturation
$S_{e[w]}$	effective water saturation
S_n	LNAPL saturation
S_{ni}	initial LNAPL saturation
S_{nr}	LNAPL residual saturation
S_{NWr}	non-wetting phase residual saturation
$S_{n/aw}$	spreading coefficient for LNAPL across air-water interface
S_w	water saturation
S_W	wetting phase saturation
S_{wi}	initial water saturation
S_{wr}	irreducible water saturation
S_{Wr}	wetting phase residual saturation
T_n	LNAPL-layer transmissibility
U_n	LNAPL unit flux
U_w	water unit flux
W_T	width of LNAPL lens extending away from the recovery trench
z	elevation
z_{an}	air-LNAPL interface elevation in monitoring well
z_{aw}	water table elevation
z_{FGZ}	elevation of facies interface with fine-grain-zone
z_{gs}	ground surface elevation
z_{max}	maximum elevation of free LNAPL (due to capillary rise)
z_{nw}	LNAPL-water interface elevation in monitoring well
z_r	reference elevation
z_{wt}	elevation of water table
z_{12}	elevation of interface between soil layers 1 and 2
z_{23}	elevation of interface between soil layers 2 and 3

α	van Genuchten α parameter
α_{an}	vG-α air-LNAPL scaling relationship for interfacial tension plus buoyancy
$\alpha_{[an]}$	vG-α air-LNAPL scaling relationship for interfacial tension
α_{nw}	vG-α LNAPL-water scaling relationship for interfacial tension plus buoyancy
$\alpha_{[nw]}$	vG-α LNAPL-water scaling relationship for interfacial tension
β	recoverable volume slope parameter
η	LNAPL transmissibility slope parameter
θ_c	contact angle
λ	Brooks and Corey pore size distribution index
μ	dynamic viscosity
μ_a	air dynamic viscosity
μ_n	LNAPL dynamic viscosity
μ_r	LNAPL-water viscosity ratio ($\mu_r = \mu_n/\mu_w$)
μ_w	water dynamic viscosity
ξ	LNAPL transmissibility intercept parameter
ρ_a	air density
ρ_n	LNAPL density
ρ_r	LNAPL-water density ratio ($\rho_r = \rho_n/\rho_w$)
ρ_w	water density
σ_{an}	air-LNAPL surface tension
σ_{aw}	air-water surface tension
σ_{nw}	LNAPL-water interfacial tension
χ	recoverable volume intercept parameter

EXECUTIVE SUMMARY

This document provides background information necessary to characterize the behavior of LNAPL in porous media with regard to performance of LNAPL liquid recovery technologies. The scope of information is selected to support model assumptions and development for the API LNAPL Distribution and Recovery Model (LDRM) which simulates the performance of proven hydraulic technologies for recovering free-product petroleum liquid releases to groundwater. This manuscript (Volume 1) and its companion manuscript (Volume 2) supplement API Publication Number 4682 and 4729, and document the LDRM software models for design and analysis of liquid free-product recovery systems using single- and dual-pump wells, vacuum-enhanced wells, skimmer wells, and trenches.

The scenario-based models for recovery wells and trenches are described in Section 1. Section 2 provides necessary background information for characterizing the vertical distribution of LNAPL located near the water table under conditions of vertical equilibrium. Capillarity, capillary pressure curves, and LNAPL residual saturation are discussed. The capillary pressure curve model presented by van Genuchten is presented, along with scaling relationships that allow the model representation to be applied with different multiphase fluid systems. Hubbert's relationships for forces in multiphase fluid systems are presented. These are important in understanding how water-enhanced and vacuum-enhanced recovery systems create hydraulic gradient within the LNAPL phase causing its movement to a well or trench. The relationship between LNAPL thickness in a monitoring well and fluid pressure and capillary pressure within a formation is discussed in some detail. This relationship, when combined with a capillary pressure curve model, allow one to estimate LNAPL accumulations within the porous medium from monitoring well thickness measurements. Significant parameters are identified. Calculation of LNAPL specific volume and LNAPL recoverable volume as a function of LNAPL thickness in a well is discussed.

Section 3 concerns possible LNAPL movement. Darcy's law is presented for LNAPL flow, and the Burdine and Mualem LNAPL relative permeability models are discussed. The effect of vertical hydraulic gradient in fine-grain soil on LNAPL saturation is described, and the critical vertical gradient at which LNAPL is displaced to accumulate beneath fine-grain soil is identified. Potential lateral migration of LNAPL is discussed. For lateral migration into pristine soils, capillary pressure curve models that include a finite displacement pressure should be used, and it is shown that LNAPL plumes are stable towards lateral spreading (an LNAPL plume will stop spreading even though LNAPL has a positive head). The vertical distribution of LNAPL mobility ratio is examined to show LNAPL is much more mobile in the upper part of the capillary fringe than groundwater. The LNAPL-layer transmissibility is introduced to calculate the LNAPL-layer volume flux. The lateral flow equations for LNAPL to wells and trenches are developed for water-enhanced and vacuum-enhanced systems, and for skimmer wells.

Section 4 shows how the continuity principle applied with regions of capture can be used, when combined with the LNAPL recoverable volume and transmissibility functions, to predict performance of LNAPL liquid recovery systems. Model parameterization and integration are discussed, and the basic equations of LDRM are presented.

1 INTRODUCTION

1.1 BACKGROUND AND OBJECTIVES

The American Petroleum Institute (API) Publication Number 4682, *Free-Product Recovery of Petroleum Hydrocarbon Liquids* (Charbeneau et al., 1999), provides an overview of recovery technologies for petroleum hydrocarbon liquids that are released to the subsurface environment and accumulate near the water table. The primary recovery technologies include skimmer wells that produce hydrocarbon liquids and single- and dual-pump wells that produce both water and hydrocarbon liquids. Hydrocarbon liquid recovery rates may also be enhanced by applying a vacuum pressure to the well to increase the gradient towards the well within the hydrocarbon layer. API 4682 describes two (Excel spreadsheet) models that may be used to characterize the subsurface distribution of liquid hydrocarbon (lighter-than-water nonaqueous phase liquids, LNAPL) in a single homogenous soil layer and to calculate the potential recovery rate and time using single- and dual-pump wells, and vacuum-enhanced wells.

API Publication Number 4729, *Models for Design of Free-Product Recovery Systems for Petroleum Hydrocarbon Liquids* (Charbeneau, 2003) describes scenario-based models for LNAPL liquid recovery using skimmer wells, water and vacuum enhanced recovery wells, and trenches. Soil capillary pressure characteristics are described using the van Genuchten (1980) capillary pressure model (soil characteristics and LNAPL distribution are described in API 4682 using the Brooks and Corey (1964) capillary pressure model). Implementation of the models through use of four separate spreadsheets is presented, based on single or two-layer heterogeneity, and on selection of relative permeability model (Burdine, 1953, or Mualem, 1976).

The present documentation supports release of the *LNAPL Distribution and Recovery Model (LDRM)* by API which supersedes API 4682 and API 4729 through development of a more general modeling framework with up to three soil layers. The objective of the present manuscript (Volume 1) is to provide necessary background information to support modeling assumptions and development of scenario-based models describing LNAPL liquid recovery. The scope of the material presented documents the quantitative framework on which the LNAPL distribution and recovery model is based. A more general discussion of LNAPL topics is presented in the *API Interactive LNAPL Guide* (2004). Huntley and Beckett (2002) discuss the effects of LNAPL recovery on dissolved plumes. Model implementation through a single executable program and model testing are described in a companion document (Volume 2).

1.2 SCENARIOS FOR FREE-PRODUCT HYDROCARBON LIQUID RECOVERY

Proven technologies for free-product recovery of petroleum hydrocarbon liquids are described in API 4682. Models to provide quantitative estimates of system performance must necessarily be based on simplifying assumptions that will not be applicable to all field conditions. Nevertheless, the models provide insight and guidance that should be helpful in technology selection and system design, and in analysis of system performance. The model scenarios for well systems and trenches are discussed separately.

For this model formulation, the subsurface porous media is assumed to be laterally homogeneous, but can have up to three distinct layers (numbered with Layer 1 on top) with different soil characteristic and permeability parameters. The vertical transition between layers is assumed to be abrupt. An example two-layer soil system is shown in Figure 1.1. This figure shows a monitoring well with an LNAPL layer located between the air-NAPL interface z_{an} and the NAPL-water interface z_{nw}. The total monitoring well LNAPL thickness is b_n. The elevation of the abrupt transition between the upper and lower soil layers is designated z_{12}. The elevation of the water table is designated z_{aw}. While the water table is not present because of the LNAPL layer, its elevation is easily determined from the elevations z_{an} and z_{nw}, and the LNAPL density ρ_n (see Section 2).

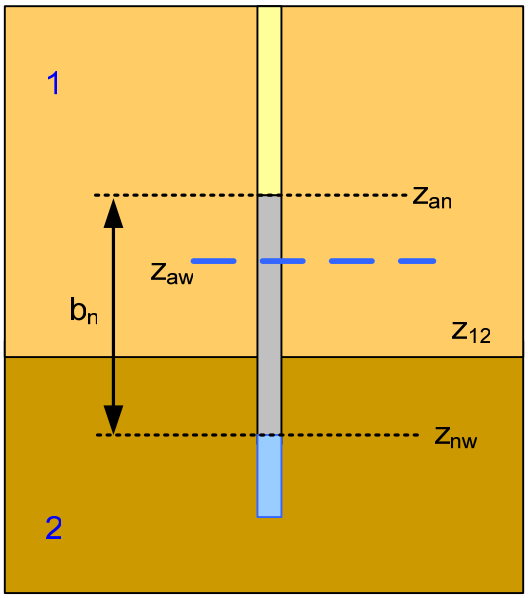

Figure 1.1—Monitoring well LNAPL thickness, b_n

The soil texture characteristics that must be defined for each layer of the porous medium include the porosity n; the (water phase) hydraulic conductivity K_{ws}; the van Genuchten parameters N and α; and the irreducible water saturation, S_{wr}. Selection of residual LNAPL saturation values remains an elusive issue, and various options are described in Section 2. Fluid properties include the LNAPL density, ρ_n (it is assumed that the water density is 1 g/cm^3), and the water and LNAPL surface and interfacial tensions, σ_{aw}, σ_{an}, and σ_{nw}.

1.2.1 Scenarios for Recovery Well Systems

The basic scenario for free-product recovery using well systems is the same for single- and dual-pump wells, vacuum-enhanced wells, and skimmer wells. The performance of each well is characterized in terms of its radius of capture R_c, with a typical scenario shown in Figure 1.2. This figure depicts a plan view of an LNAPL lens (in gray color) with 7 recovery wells located so that the pattern of wells with their radius of capture will cover most of the area of the lens. For single- and dual-pump well systems, the radius of capture could extend out to the radius of influence (water production) of the well. For vacuum-enhanced systems, the radius of influence of the vacuum extraction well (which, because of air leaking from the ground surface, is

typically on the order of 30 feet – 40 feet) limits the radius of capture. For skimmer wells, the radius of capture is also limited to probably 10 feet – 30 feet, depending on the soil characteristics.

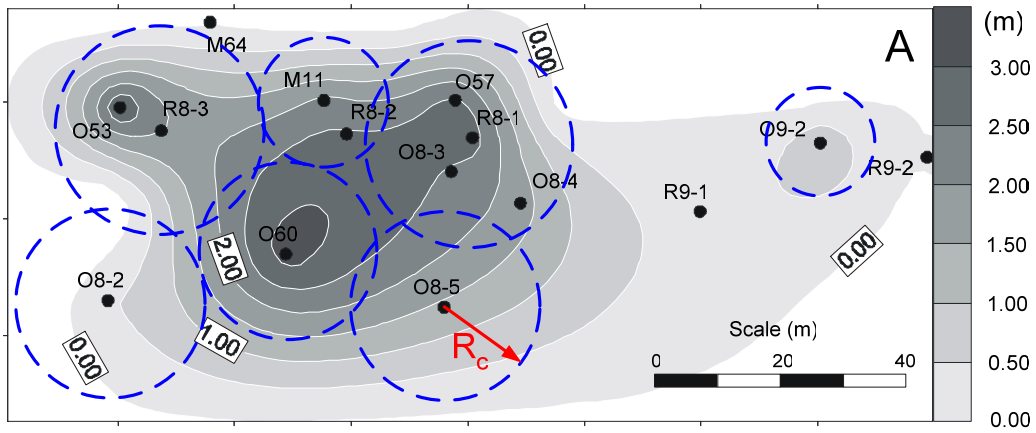

Figure 1.2—Recovery well system with 7 recovery wells showing the radius of capture (modified from Lefebvre, 2000)

The data required for analysis of recovery-well-system performance includes the radius of capture for the well, the LNAPL-water viscosity ratio μ_r (the water viscosity is assumed to be 1 cp), and water production rate for a water-enhanced system or wellhead vacuum pressure for a vapor-enhanced system. For a water-enhanced system, the effective depth of penetration of the well into the aquifer must be specified, while for a vacuum-enhanced system, the screened interval of the vadose zone must be given. The effective relative permeability of the vadose zone due to the presence of residual soil water is assumed to be k_{ra} = 0.9. If zero water production and wellhead pressure are specified, then the well is assumed to function as a skimmer well.

1.2.2 Scenario for LNAPL Recovery Using Trenches

The modeling framework may also be used to represent a simple trench recovery system, such as shown in Figure 1.3. The trench has a length L_T transverse to the direction of groundwater flow. The LNAPL lens is assumed to be of rectangular shape with length L_T and width W_T. The natural groundwater hydraulic gradient J_w is transferred to the LNAPL layer and carries it into the trench where LNAPL is removed by skimmer wells or other technology. The rate of LNAPL discharge into the trench will depend on the effective lens thickness as observed in a monitoring well, soil texture, natural groundwater hydraulic gradient, and whether groundwater is also produced from the trench in order to increase the hydraulic gradient. If the trench cuts across an LNAPL lens, then the upstream and downstream sections of the lens must be analyzed separately, with J_w being negative on the downstream side.

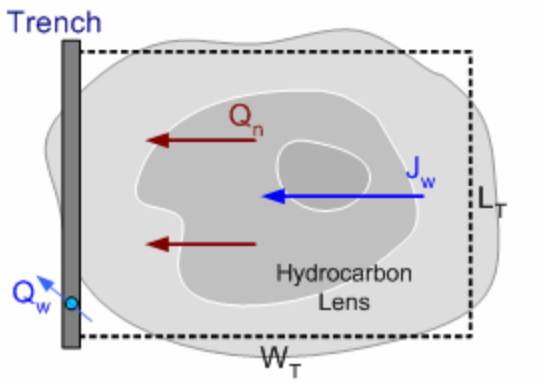

Figure 1.3—Simple Trench System for LNAPL Recovery

1.3 OVERVIEW

The models for well and trench recovery systems provide estimates of the recovery volume and rate as a function of time. The mathematical models on which these estimates are based use a simple representation of the LNAPL layer effective saturation and transmissibility. The representation is consistent with the actual formation distributions of LNAPL saturation and relative permeability under conditions of vertical equilibrium, and within the modeling framework, balance of LNAPL volume (continuity) is maintained between the recovered volume and formation LNAPL volume within the well radius of capture or lens rectangular area. Section 2 discusses the effects of capillarity on LNAPL in porous media and the relationship between monitoring well LNAPL thickness and formation LNAPL saturation distribution. The quantity of LNAPL is characterized through functions representing the LNAPL specific volume (integral of the LNAPL volumetric content over the lens thickness) and recoverable specific volume, as a function of monitoring well LNAPL thickness. A key to model simplicity is representation of these relationships through piecewise linear functions.

Section 3 discusses LNAPL relative permeability as a function of multiphase saturation. Both the Burdine (1953) and Mualem (1976) models are used. When combined with the soil hydraulic conductivity, vertical integration of the LNAPL relative permeability distribution is used to characterize lateral movement through the resulting transmissibility function. LNAPL transmissibility is also represented as a piecewise linear function of monitoring well LNAPL thickness.

The mathematical models for predicting free-product recovery are developed in Section 4. These models are based on the free-product thickness that one would observe in a monitoring well in good communication with the formation fluids (water, LNAPL, air). The rate equations for single- and dual-pump wells, vacuum-enhanced wells, skimmer wells, and trench recovery systems depend on the monitoring well LNAPL thickness and on the discharge of formation fluids (water or air). The principle of continuity is applied to predict how the monitoring well LNAPL thickness (and recovery rate) varies as a function of time.

2 LNAPL DISTRIBUTION

The purpose of this section is to provide background information on LNAPL behavior in the subsurface environment. This background information is necessary for understanding the distribution of LNAPL liquids under conditions of vertical equilibrium. It includes the effects of capillary forces on the distribution of immiscible fluids in porous media and methods for predicting the formation LNAPL saturation distribution as a function of monitoring well LNAPL thickness. Representation of LNAPL residual saturation is also discussed. Additional information on the effects of capillarity on the behavior of multiphase fluids in porous media may be found in Bear (1972), Corey (1986), and Dullien (1992).

2.1 CAPILLARITY IN POROUS MEDIA

2.1.1 Surface Tension, Wettability and Capillary Pressure

When the pore space of a porous medium is occupied by two or more immiscible fluids, the interface separating fluid phases is the most significant feature. Molecules near this interface have greater energy than molecules within the bulk phase, and the excess interfacial energy makes the interface act as a membrane under tension; the total energy in the system is minimized through minimizing the interfacial area (Hillel, 1980). The source of the interfacial energy (or surface tension) is associated with the attractive forces that exist between molecules in the liquid phase. For molecule *A* within the bulk liquid phase-β shown in Figure 2.1, it is attracted equally by neighboring molecules on all sides, resulting in no net force on the molecule associated with molecular attraction. Now consider the molecule at location *B* shown in this figure. It is attracted by neighboring molecules within the bulk phase but not by those in the phase-α [if molecules in phase-α also attracted the molecule from phase-β, then the interface would not exist and the phases would be miscible]. There is a net force on the molecule located at *B*. In order for molecules at locations *A* and *B* to change places, the molecule from *A* would have to move against this force field, thus gaining energy. Likewise, the molecule from *B* would move in the direction of the net force, loosing energy. Thus molecules near the interface must have greater energy than molecules within the bulk phase. This interfacial energy (per unit area, erg/cm^2) is the same as the surface tension (dyne/cm), and results in capillary phenomena trying to minimize the interfacial area (minimize the free energy of the system at equilibrium).

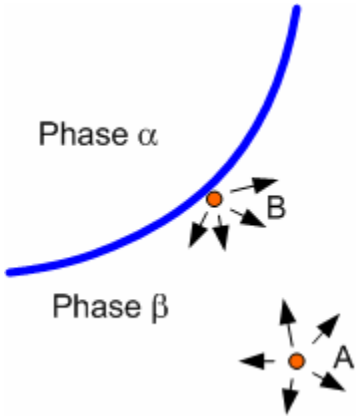

Figure 2.1—Interfacial energy associated with molecular attraction in the liquid phase

Along lines of contact of the interface with a solid phase, the interface will make a contact angle, θ_c. The phase with the smaller contact angle preferentially covers the surface, and is called the wetting phase. The contact angle is the angle measure between the solid surface and the interface through the wetting phase, as shown in Figure 2.2. For usual field conditions of interest in environmental investigations, the *wettability* sequence mineral based soil is water → NAPL → air, with water being the most wetting phase for mineral porous media.

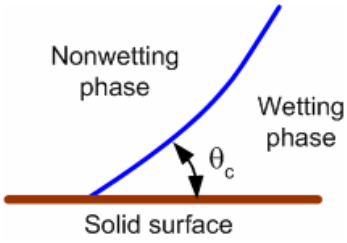

Figure 2.2—Contact angle and wettability

If the interface separating two fluid phases is curved, then there will be a pressure difference across the interface between the phases on either side. This pressure difference is called the *capillary pressure*, and it depends on the interfacial energy (surface tension), contact angle, and mean radius of curvature. The capillary pressure is the excess pressure in the nonwetting phase over the wetting phase, and it may be calculated using the equation of Young (1805) and Laplace (1806) as follows (Adamson, 1982):

$$p_c = \frac{2\sigma\cos(\theta_c)}{\bar{r}} \tag{2.1}$$

In equation (2.1), p_c is the capillary pressure, σ is the surface tension (interfacial energy), and $\bar{r}$ is the mean radius of curvature of the interface. In a water-wet porous medium, excess pressure must be applied to the nonwetting phase (air or NAPL) to displace water from the medium, and the capillary pressure is positive. It is assumed that the radius of the pore containing the interface between wetting and nonwetting fluid is the same as the mean radius of curvature.

2.1.2 Capillary Pressure Curves

An important characteristic of a porous medium is the relationship between the capillary pressure and wetting fluid saturation (Hillel, 1980). This characteristic is called the *capillary pressure curve* (and it is so important, it is often simply called the "characteristic curve" for the soil). Increases in capillary pressure will force the interfaces between the nonwetting and wetting phase into smaller pore spaces (equation 2-1), and result in a corresponding increase in nonwetting phase saturation and decrease in wetting phase saturation. Likewise, decreases in capillary pressure will allow the interface to move into larger pore spaces, with an increase in wetting phase saturation and decrease in nonwetting phase saturation. Because of the complex system of pore spaces, the sequence upon drainage of pore space is not the same as that upon re-filling, and the capillary pressure curve shows *hysteresis*. This means that the relationship between capillary pressure and saturation is not a single function, but will also depend on the wetting and drainage history of the soil.

The capillary pressure curve is usually measured by starting with a soil that is fully saturated with wetting phase fluid. A nonwetting fluid is introduced at increasing capillary pressures. Time is provided for the fluids to equilibrate within the pore space, and the resulting saturation values are recorded. The capillary pressure is increased until no further reduction in wetting phase saturation is measured. The end-point value is the *wetting-phase residual saturation*, S_{Wr}, and represents the wetting phase fluid that is held tightly at grain contacts and as fluid skins, so that the wetting phase is no longer continuous for flow. The resulting capillary pressure versus saturation curve is called the *drainage curve*. It provides a measure of initial displacement of wetting phase by nonwetting phase. The drainage curve is usually used to characterize the soil.

If the experiment described in the preceding paragraph is continued, with the capillary pressure being lowered starting with wetting-phase residual saturation, then the resulting saturation versus capillary pressure values follow the *imbibition curve*. When the capillary pressure is lowered to zero, the soil will not be fully saturated with the wetting phase fluid. This end-point nonwetting phase saturation is sometimes called the *nonwetting-phase residual saturation*, S_{NWr} (though this concept requires further discussion for practical field applications, see below). Figure 2.3 shows a graphical representation of the experiment that has been described. Both the primary drainage and wetting curves are shown. If the drainage-imbibition cycle is stopped and reversed before the residual endpoints are reached, then a *scanning curve* results. Two such curves are also shown in Figure 2.3.

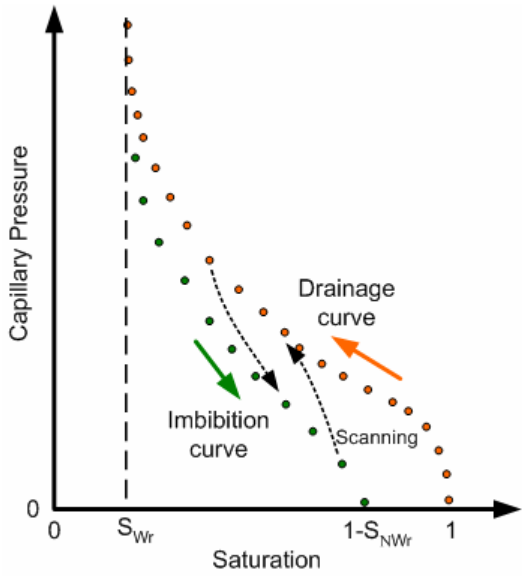

Figure 2.3—Soil capillary pressure curve showing primary drainage, imbibition, and scanning characteristic curves

2.1.3 Residual LNAPL Saturation

The nonwetting phase residual saturation shown in Figure 2.3 is a reproducible measure of the capacity of a porous medium to retain nonwetting fluid during re-filling with the wetting phase for a two-phase fluid system. However, such values have little relevance to issues associated with LNAPL in the groundwater environment (Adamski et al., 2003). Typical LNAPL releases result in LNAPL-water capillary pressures which are very much smaller than those required to

produce irreducible water saturations along the primary drainage curve. Most often, maximum LNAPL saturation values observed in the field are less than LNAPL residual values suggested using the experimental procedure suggested by Figure 2.3. Thus many of the literature-reported tabulated values of residual LNAPL saturation are of limited use in environmental remediation applications. For example, an often cited reference is Mercer and Cohen (1990) who report residual LNAPL saturation values ranging from 0.15 to 0.50 for the saturated zone, and 0.10 to 0.20 for the vadose zone. These values are much larger than the maximum LNAPL saturation values measured at industrial facilities with appreciable LNAPL contamination issues (Mark Adamski, BP America, personnel communication, 2004). To be useful, estimates of LNAPL residual saturation must consider the nature of the LNAPL release and the maximum LNAPL saturation values that exist under field conditions.

A typical field situation of an LNAPL release is outlined in Figure 2.4. The location is assumed to be near the water table, and the porous medium is initially saturated with water. As released LNAPL accumulates near the water table, it will develop a pressure greater than that of the neighboring groundwater (positive capillary pressure) and displace water from the medium following the drainage curve. Point *A* in Figure 2.4 corresponds to the maximum capillary pressure developed by the LNAPL release and results in an 'initial' LNAPL saturation $S_{ni} = 1 - S_{wi}$. Here, the term "initial" refers to the beginning of the recovery period where water displaces LNAPL from the medium, with capillary pressure-saturation following a scanning curve. During LNAPL recovery, at point *B* in the figure, the capillary pressure has been reduced to zero and LNAPL will no longer move into a recovery well due to a capillary pressure driving force. The remaining LNAPL saturation, designated S_{nr}, cannot be recovered using conventional LNAPL hydraulic recovery technologies. The fraction S_{nr} represents the LNAPL remaining trapped within the formation.

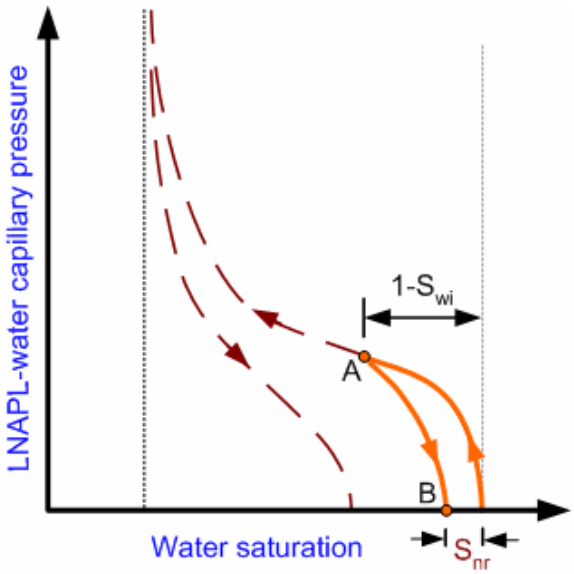

Figure 2.4—LNAPL residual saturation under normal field conditions

While limited theory exists to predict residual LNAPL saturation values, S_{nr}, from initial saturation values $(1 - S_{wi}) = S_{ni}$, there is sufficient empirical data to develop useful predictive models. Data from laboratory column experiments, shown in Figure 2.5, suggests that residual

LNAPL saturation values increase with initial LNAPL saturation. These experimental results from Kueper et al. (1973) were for TCE (DNAPL) in a sand-packed column.

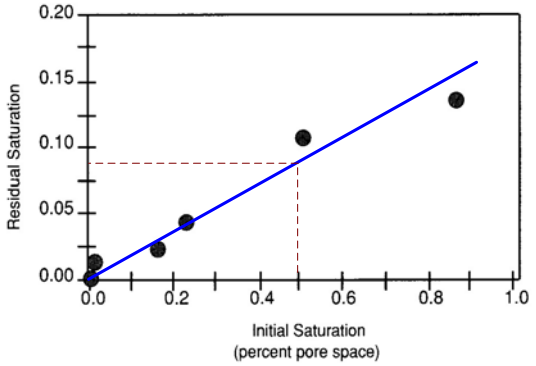

Figure 2.5—LNAPL residual saturation increases with initial LNAPL saturation (after Kueper et al., 1993)

Figure 2.6 from Johnston and Adamski (2005) shows experimental data from laboratory retention cell studies with capillary pressure cycled to increasing values and then returned to zero. The Safety Bay Sand data is from Steffy et al. (1997). The other data is from more recent studies carried out in CSIRO laboratories in 2004 and 2005.

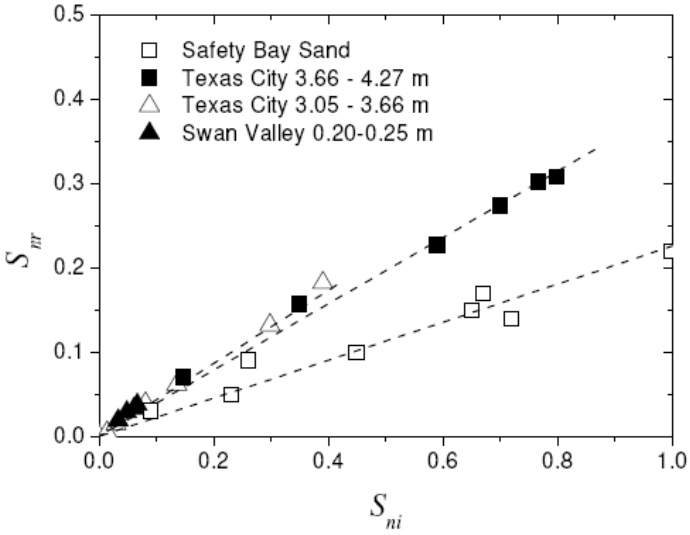

Figure 2.6—LNAPL residual saturation depends on initial LNAPL (from Johnston and Adamski, 2005)

Data from these and other experiments suggests that LNAPL residual saturation values increase linearly with increasing initial LNAPL saturation. This means that regions that accumulate greater LNAPL saturations during a release will retain greater LNAPL residual saturations during subsequent migration and recovery.

The suggested mathematical model relating initial and residual saturations is

$$S_{nr} = f_r \left(1 - S_{wi}\right) = f_r \, S_{ni} \tag{2.2}$$

The residual f-factor appears to vary with soil texture, and may also vary for the saturated (two-phase) and vadose (three-phase) zones. Figure 2.5, for a two-phase system with Ottawa sand, gives f_r = 0.18. For the Safety Bay Sand (fine-to-medium sand), the data shown in Figure 2.6 give f_r = 0.23. For the Texas City soils shown in this figure, which are a fine-sand (SP-SC) and loamy sand (SC), the laboratory experiments give f_r = 0.39 and 0.43, respectively. For the Swan Valley clay loam (CL), f_r = 0.56.

A predictive model form similar to equation (2.2) is suggested by Waddill and Parker (1997), where they interpret S_{wi} as the "quasi-static" residual saturation accounting for small but residual water movement in the unsaturated zone. For the vadose zone their model predicts that the f-factor is smaller by an amount also dependent on the initial LNAPL saturation [$f_{rv} = f_{rs} \, (1 - S_{ni})$]. Waddill and Parker suggest empirical f-factor values ranging between 0.2 and 0.5, and recommend a median value of 0.3.

2.1.4 Spreading Coefficients

With LNAPL present at the interface between air and water, the spreading coefficient measures the tendency of for LNAPL to spread on water (Adamson, 1982; Dullien, 1992). The spreading coefficient $S_{n/aw}$ may be defined by (see Figure 2.7)

$$S_{n/aw} = \sigma_{aw} - \left(\sigma_{an} + \sigma_{nw}\right) \tag{2.3}$$

The significance of the spreading coefficient may be appreciated if one considers the surface and interfacial tension values as "surface energy." As noted earlier, molecules near the surface of a liquid have excess energy compared with molecules within the bulk liquid phase. At equilibrium, the porous medium (fluid phases plus solid) will achieve a state of least (free) energy. This implies that if the spreading coefficient is negative ($S_{n/aw} < 0$), then the LNAPL drop will remain stable on the air-water interface, forming a "bead" such as shown in Figure 2.7. This distribution would minimize the total surface energy. On the other hand, if the spreading coefficient is positive, then the drop will spread over the interface resulting in a layer (film) of LNAPL existing between the water and air phase. This condition will also result in a state of minimum free energy for a positive spreading coefficient.

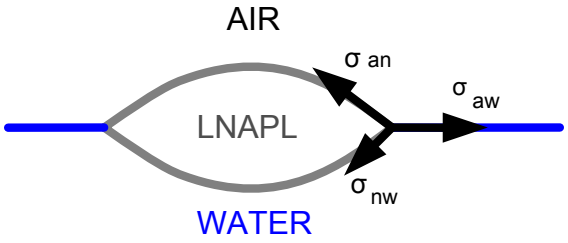

Figure 2.7—LNAPL drop located on an air-water interface

For most LNAPL systems the spreading coefficient is positive, and within the vadose zone, LNAPL is in direct contact with the air phase. This leads to Leverett's assumption (discussed below). There is question as to whether the spreading coefficient will influence the residual LNAPL saturation in the vadose zone. It is possible that a spreading LNAPL phase will allow downward migration of LNAPL through film-flow, resulting in lower LNAPL-residual saturation values. Zhow and Blunt (1997) provide experimental data suggesting that three-phase LNAPL residual saturation values can be very low (less than 0.1%) for fluid systems with positive spreading coefficients.

2.1.5 Leverett Assumptions

Based on results from his research on capillarity in porous media, Leverett (1942) suggests that within a three-phase fluid system, 1) the capillary pressure between the water and NAPL phase depends only on the water saturation, while 2) the capillary pressure between the NAPL and air phase depends on the total liquid saturation (water plus NAPL). The basis for this assumption may be appreciated through consideration of Figure 2-11, which is discussed below. Leverett specifically states that "the oil must spread on the water for this assumption to be completely valid" (positive spreading coefficient).

2.2 CAPILLARY PRESSURE CURVE MODELS

Capillary pressure curve measurements are most often fit to mathematical models that are used for quantitative analysis. For this purpose the primary drainage curve is analyzed. At present, the most popular model for environmental investigations was developed by van Genuchten (1980). This model takes the mathematical form (vG model)

$$S_e = \left(1 + (\alpha h_c)^N\right)^{-M} \tag{2.4}$$

In equation (2.3), S_e is the effective (wetting-phase) saturation that is scaled to range from 0 → 1 and h_c is the *capillary pressure head*. The model parameters are α, N and M. While N and M can be treated independently, they are most often related based on the selected model for relative permeability. If the Burdine (1953) relative permeability model is selected, then the relationship is

$$\textit{Burdine}:\ M = 1 - 2/N \quad ; \quad N > 2 \tag{2.5}$$

If the Mualem (1976) model formulation is used, the relationship is

$$\textit{Mualem}:\ M = 1 - 1/N \quad ; \quad N > 1 \tag{2.6}$$

Relative permeability functions are discussed in Section 3.1.2.
For the primary drainage curve of Figure 2.3, the effective saturation would be defined by

$$S_e = \frac{S_W - S_{Wr}}{1 - S_{Wr}} \tag{2.7}$$

Other scaling factors for the effective saturation are introduced below for the imbibition curve.

The parameters α and N may be used to characterize soil texture. Smaller values of α, which has units of length^{-1}, correspond to smaller pore sizes. Smaller values of N correspond to wider ranges in pore sizes. Together, the parameters α and N attempt to describe the pore size

distribution for the medium. The model fit (Mualem) for a fine-grain plastic clay soil with air displacing water gives $\alpha = 0.17\ ft^{-1} = 0.0056\ cm^{-1}$, $N = 1.46$, and $S_{wr} = 0.69$ is shown in Figure 2.8. Even at one-atmosphere capillary pressure (~30 ft), this soil still has more than 80% wetting-phase (water) saturation.

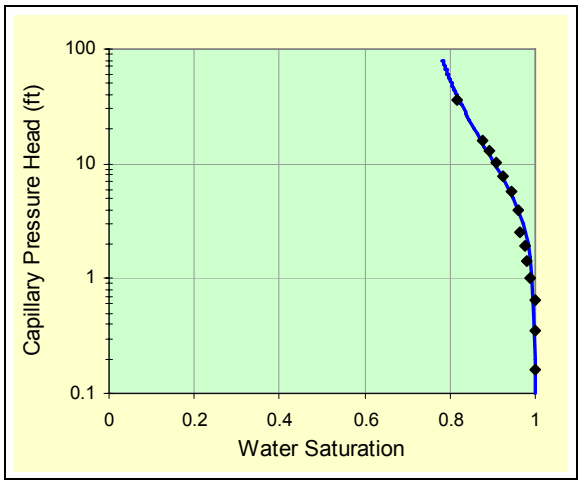

Figure 2.8—Measured capillary pressure curve

2.2.1 Fitting Models to Capillary Pressure Curve Data

Data provided through measurement of capillary pressure curves is fundamental to prediction of LNAPL behavior. Alternative methods for parameter estimation are available. A widely used, publicly available model is RETC, developed by the U.S. Salinity Laboratory (van Genuchten et al., 1991). This model is available through the web site:

http://www.ussl.ars.usda.gov/models/retc.HTM

Alternatively, simple spreadsheet models can be written to estimate capillary pressure curve parameters from measured data. An important point is that estimated values of the vG-parameters α and N will depend not only on the measured data, but also on the relative permeability model selected, equations (2.5) and (2.6). For example, Figure 2.9 shows the fitted curves and model parameters for the same data set with the Burdine and Mualem models.

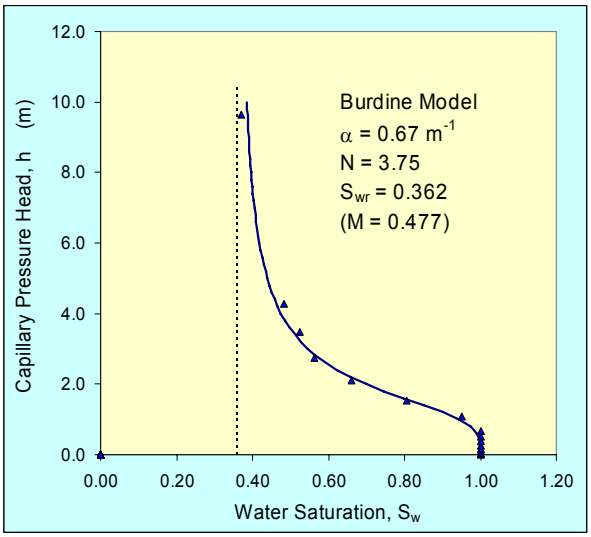

(a)

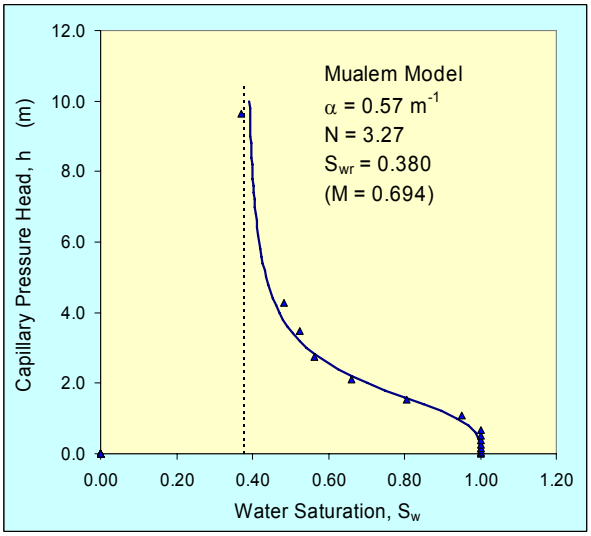

(b)

Figure 2.9—Fitted capillary pressure curve models using (a) Burdine and (b) Mualem relations

2.2.2 Pore-Size Distribution Curves

Capillary pressure models such as equation (2.4) are ideally suited for characterizing the range of drainable pore sizes of a porous medium. Using equation (2.1) to relate the pore size to the capillary pressure, then the fraction of pores of a given size may be specified by

$$p(r_c) = \frac{dS_e}{dr_c} = \frac{M\,N}{\alpha\,\beta}\,\frac{y^{N+1}}{\left(1+y^{N}\right)^{M+1}} \tag{2.8}$$

In equation (2.8), $p(r_c)$ is the fraction (probability) of pores of size r_c, r_c is assumed to equal the mean radius of curvature in equation (2.1), and $y = \alpha\beta/r_c$ where $\beta = 2\sigma\cos(\theta_c)/(\Delta\rho g)$. An equivalent expression to equation (2.8) was introduced by Drake and Ritter (1945). Graphs of $p(r_c)$ for two different soils are shown in Figure 2.10 (the area under each curve is one). The

median pore size varies from a few microns to more than 100 microns for these two examples. In general, one finds that increasing the value of α shifts the curves to larger pore sizes (including the size of the largest pores). If the value of the parameter N is increased, the range in pore sizes decreases (the distribution becomes narrower). Thus the parameter α is associated (directly) with the size of pores while the parameter N is associated (inversely) with the range in pore size.

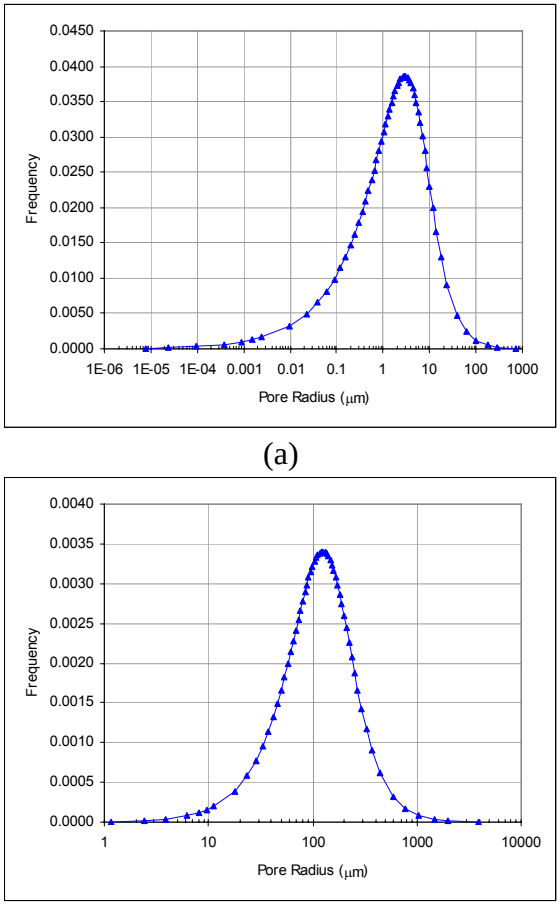

Figure 2.10—Pore size distribution curves from equation (2.8) for (a) fine-grain soil with α = 0.15 ft^{-1} (0.005 cm^{-1}), N = 1.5; and (b) fine sand soil with α =3.8 ft^{-1} (0.125 cm^{-1}) N = 2.5

When combined with the concept of wettability, the notion of distribution of pore sizes allows one to understand a number of significant characteristics of multiphase porous media behavior. According to the concept of wettability, the wetting phase will occupy the smallest pore sizes while the nonwetting phase will occupy the largest. This distribution is shown schematically in Figure 2.11. Characteristics such as permeability may be associated with pore size. Thus when associating relative permeability with fluid saturation, one should associate the larger pore sizes for the nonwetting phase and the smaller pore sizes for the wetting phase.

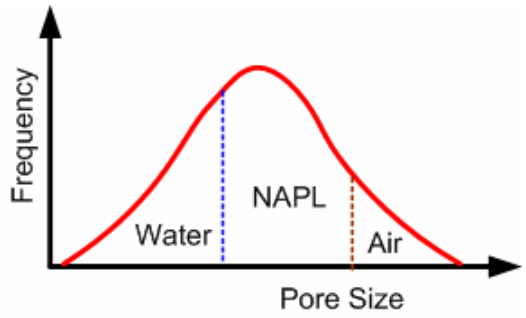

Figure 2.11—Distribution of fluid saturation among various pore sizes

2.2.3 Capillary Scaling Relationships

Measurements of capillary pressure curves are made for a single fluid-pair system, usually the air-water system for environmental applications. An important question is how to scale parameters that have been determined for one fluid system to a different fluid combination. In this regard, interpretation of the physical significance of parameters is important. With regard to the vG-model of equation (2.2), the *parameter* α is associated directly with the capillary pressure head. Using equation (2.1) for guidance, it appears that scaling relationships should include the surface tension and contact angle ratios.

The *parameter N* is associated with the pore size distribution. It is assumed that the distribution of pore sizes does not change for different fluid systems; that is, there is neither significant shrinkage nor swelling of the porous medium for different fluid systems. For this case, the parameter *N* will not change for different fluid combinations. Thus the capillary scaling relationships must consider only the parameter α.

Assuming that the α value was obtained for an air-water system, the appropriate scaling relationships for the NAPL-water and air-NAPL system are

$$\alpha_{[nw]} = \frac{\sigma_{aw}}{\sigma_{nw}} \alpha \tag{2.9}$$

$$\alpha_{[an]} = \frac{\sigma_{aw}}{\sigma_{an}} \alpha \tag{2.10}$$

Use of these scaling parameters along with the appropriate capillary pressure heads for the different fluid systems will assure that capillary pressure-fluid saturation relation is conserved for different fluid pairs. With regard to the pore size distribution curve, this means that the interface between wetting and nonwetting fluids would be located within appropriate pore size based on capillary pressure, regardless of the fluid-pair combination.

2.3 FORCES IN MULTIPHASE FLUID SYSTEMS

Newtonian fluids (water, NAPL, air) will not move unless there is force acting on them. The principle forces causing fluid movement are pressure gradients and gravity. If there is a balance between the vertical pressure gradient and gravity in each fluid phase, then a condition of hydrostatics (*vertical equilibrium*) exists, and there will be no motion in the vertical direction.

Even under conditions of vertical equilibrium, there can be lateral gradients resulting in (primarily) horizontal fluid movement.

The force per unit weight acting within each phase is called the *hydraulic gradient* (dimensionless). For the water and NAPL phases, both pressure gradients and gravity are important. However, for air, because of its small density, gravity forces are small and are neglected in calculation of the hydraulic gradient (*J*). For the three phases, the hydraulic gradients are specified by

$$\vec{J}_w = -\frac{\nabla p_w}{\rho_w g} - \hat{k} \tag{2.11}$$

$$\vec{J}_n = -\frac{\nabla p_n}{\rho_n g} - \hat{k} \tag{2.12}$$

$$\vec{J}_a = -\frac{\nabla p_a}{\rho_a g} \tag{2.13}$$

Equations (2.11) and (2.12) may be combined using the definition of the capillary pressure between LNAPL and water ($p_{c[nw]} = p_n - p_w$) to give (Hubbert, 1953)

$$\vec{J}_n = -\frac{\nabla p_{c[nw]}}{\rho_n g} + \left(\frac{\rho_w}{\rho_n} - 1\right)\hat{k} + \frac{\rho_w}{\rho_n}\vec{J}_w \tag{2.14}$$

Similarly, equations (2.12) and (2.13) may be combined using the definition of the capillary pressure between the air and LNAPL ($p_{c[an]} = p_a - p_n$) to give

$$\vec{J}_n = \frac{\nabla p_{c[an]}}{\rho_n g} - \hat{k} + \frac{\rho_a}{\rho_n}\vec{J}_a \tag{2.15}$$

Equations (2.14) and (2.15) state that the fluid forces acting on the NAPL phase consist of 1) forces due to capillary pressure gradients, which in turn depend on the soil texture distribution and the fluid saturations, 2) buoyancy, which acts upward when NAPL density is less than the water density, and 3) forces associated with water or air phase movement. When the first two terms balance (cancel), there is no vertical fluid movement. In this case LNAPL can only move laterally induced by the flow of water or air. This is one of the primary assumptions of the LNAPL recovery model.

If only the *vertical components* of the hydraulic gradients vanish, then the LNAPL-water and air-LNAPL capillary pressure distributions satisfy the following equations:

$$p_{c[nw]} = (\rho_w - \rho_n)g(z - z_{r1}) \tag{2.16}$$

$$p_{c[an]} = \rho_n g(z - z_{r2}) \tag{2.17}$$

In equations (2.16) and (2.17) the elevations z_{r1} and z_{r2} are reference elevations at which the respective capillary pressure is zero (the pressures in the nonwetting and wetting phases are the same).

2.4 LNAPL DISTRIBUTION AND MONITORING WELLS

2.4.1 Fluid Levels in Monitoring Wells

If LNAPL is present within the subsurface environment in sufficient quantify, then it may appear in monitoring wells that are screened across the water table elevation. The levels of NAPL and water in the well will adjust through time until the fluids in the well are in equilibrium (same energy) with those in the formation; differences in energy levels would cause flow into or out of the well. Figure 2.12 provides a schematic view of LNAPL in a monitoring well. The elevation z_{gs} is the elevation of the ground surface. The elevations z_{an} and z_{nw} are the elevations of the air-NAPL and NAPL-water interface in the well, respectively. z_{aw} corresponds to the elevation of the water table if no NAPL were present. b_n is the thickness of the NAPL layer in the monitoring well.

Under equilibrium conditions between fluids in the well and those within the formation, all of the variable values shown in Figure 2.12 are determined by the formation LNAPL distribution.

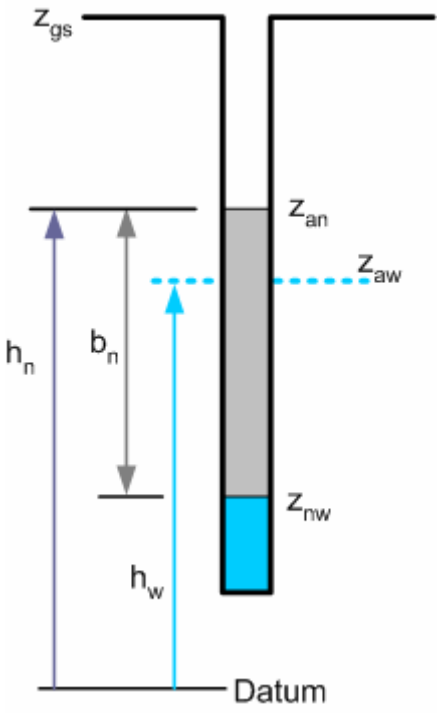

Figure 2.12—Fluid elevations within an LNAPL monitoring well

2.4.2 Distribution of Capillary Pressures

Under hydrostatic conditions, the fluid pressure in each phase changes in the vertical direction in accordance with the hydrostatic pressure equation, which expresses a balance between pressure and gravity forces. For either water or LNAPL this may be written

$$\frac{dp}{dz} = -\rho g \tag{2.18}$$

For the air phase, gravity forces are small and the equivalent equation would read $p_a = p_{atm}$ = constant, i.e. air pressure remains constant at atmospheric pressure under equilibrium conditions.

The equilibrium (hydrostatic) pressure distribution for an air-water system is shown in Figure 2.13. At the elevation of the water table (z_{aw}) the water pressure is atmospheric (gage pressure is zero). It is assumed that the air pressure remains atmospheric throughout. The height of the capillary fringe is determined by the *displacement pressure head*, h_d, of the soil. Smaller pore sizes result in a greater height of the capillary fringe. In a region that has not been impacted by LNAPL, the capillary fringe remains nearly water-saturated with negative water pressure.

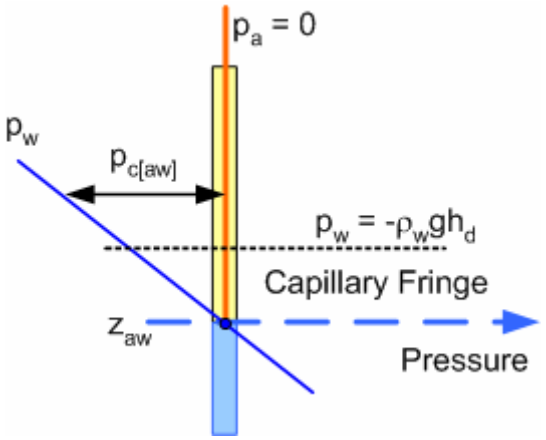

Figure 2.13—Capillary pressure distribution near the water table, including the capillary fringe

Figure 2.14 shows the capillary pressure distribution for a region impacted by LNAPL. The gage water pressure is still zero at the water table. The LNAPL pressure is zero at the elevation z_{an}. This would be the elevation of the air-LNAPL interface in a monitoring well, if one were present. Thus $z_{r2} = z_{an}$ in equation (2.17). The water and LNAPL pressures are the same at the elevation z_{nw}, at which the LNAPL-water capillary pressure vanishes. This would be the elevation of the LNAPL-water interface in a monitoring well, and $z_{r1} = z_{nw}$ in equation (2.16). The elevation z_{max} is the maximum elevation of free LNAPL due to capillary rise. Above this elevation, any LNAPL is present at residual saturation and is not mobile.

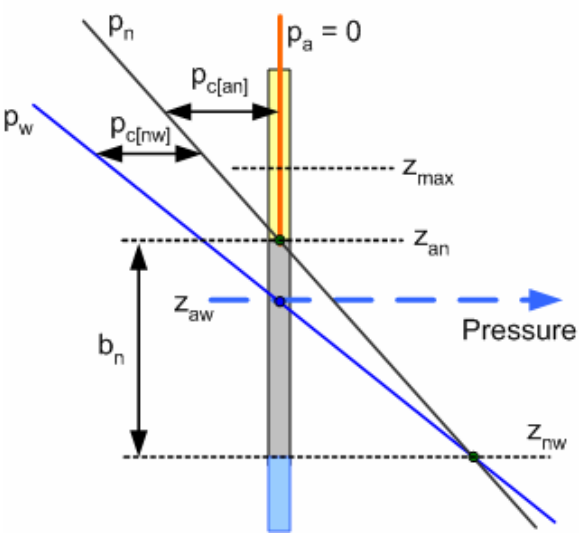

Figure 2.14—Capillary pressure distribution in the presence of LNAPL

With equilibrium conditions between the well and formation fluids, the monitoring well LNAPL thickness can be used to assess corresponding energy conditions within the formation (in general, the fluid head is specified by $h = p/\rho g + z$). This is based on knowledge of the LNAPL and water density. The following conditions are based on hydrostatic conditions within the well:

$$z_{an} - z_{aw} = (1 - \rho_r) b_n \tag{2.19}$$

$$z_{aw} - z_{nw} = \rho_r b_n \tag{2.20}$$

$$h_w = z_{aw} = \rho_r z_{an} + (1 - \rho_r) z_{nw} \tag{2.21}$$

$$h_n = z_{an} = h_w + (1 - \rho_r) b_n \tag{2.22}$$

In these equations the *density ratio*, ρ_r, is defined by $\rho_r = \rho_n/\rho_w$. Equation (2.22) is especially important because it relates LNAPL head to water head plus equilibrium LNAPL-layer thickness in a well.

2.4.3 LNAPL Saturation Distributions

Fluid level elevations in monitoring wells provide the basis, when combined with capillary pressure curves, for calculation of formation LNAPL saturation distributions (Farr et al., 1990; Lenhard and Parker, 1990). Under equilibrium conditions, the fluid energy within the well is the same as that within the formation. At the elevation z_{nw} in the well, the pressure is the same within the water and NAPL phases, and thus the capillary pressure $p_{c[nw]} = 0$ at this elevation. The elevation z_{nw} serves as the reference datum for calculation of the NAPL-water capillary pressure head distribution. According to equation (2.14) the LNAPL-water capillary pressure head distribution is given by

$$h_{[nw]} = \frac{p_{c[nw]}}{\rho_w g} = (1 - \rho_r)(z - z_{nw}) \tag{2.23}$$

Using equations (2.23) and (2.8) in equation (2.3) gives for the effective water saturation distribution in the formation

$$S_{e[w]}(z) = \left(1 + \left(\alpha_{[nw]}\, h_{[nw]}\right)^N\right)^{-M}$$

This is more conveniently written in the form

$$S_{e[w]}(z) = \left(1 + \left(\alpha_{nw}(z - z_{nw})\right)^N\right)^{-M} \tag{2.24}$$

Equation (2.24) introduces a new scaling factor that takes into account both surface tension and buoyancy effects:

$$\alpha_{nw} = (1 - \rho_r)\frac{\sigma_{aw}}{\sigma_{nw}}\alpha \tag{2.25}$$

The effective saturation in equation (2.24) accounts for the presence of residual NAPL. Thus

$$S_{e[w]} = \frac{S_w - S_{wr}}{1 - S_{wr} - S_{nr}} \tag{2.26}$$

In equation (2.26) S_{nr} is the residual NAPL saturation. With this scaling, when $S_{e[w]} = 1$, $S_w = 1 - S_{nr}$ since part of the pore space is occupied by residual NAPL. The water saturation distribution is given by

$$S_w(z) = S_{wr} + (1 - S_{wr} - S_{nr})S_{e[w]}(z) \tag{2.27}$$

In equation (2.27) both the residual water and LNAPL saturation may also vary with elevation.

For elevations $z < z_{an}$, the pore space not occupied by water will be filled with LNAPL. Thus for $z < z_{an}$,

$$S_n(z) = 1 - S_w(z) \tag{2.28}$$

In equation (2.28) the water saturation is given by equation (2.27).

In a similar fashion, one may use Leverett's assumptions and calculate the total liquid saturation above the elevation z_{an}. Using equation (2.17) the air-NAPL capillary pressure head distribution satisfies

$$h_{[an]} = \frac{p_{c[an]}}{\rho_w g} = \rho_r (z - z_{an}) \tag{2.29}$$

The total liquid effective saturation distribution is calculated using

$$S_{e[t]}(z) = \left(1 + \left(\alpha_{an}\left(z - z_{an}\right)\right)^{N}\right)^{-M} \tag{2.30}$$

In equation (2.30) the scaling coefficient is defined by

$$\alpha_{an} = \rho_r \frac{\sigma_{aw}}{\sigma_{an}} \alpha \tag{2.31}$$

The total liquid effective saturation is scaled as

$$S_{e[t]} = \frac{S_w + S_n - S_{wr} - S_{nr}}{1 - S_{wr} - S_{nr}} \tag{2.32}$$

The difference between total liquid and water effective saturation (equation 2.32 minus equation 2.36) is

$$S_{e[t]} - S_{e[w]} = \frac{S_n - S_{nr}}{1 - S_{wr} - S_{nr}}$$

Thus for $z > z_{an}$ the LNAPL saturation is given by

$$S_n(z) = S_{nr} + \left(1 - S_{wr} - S_{nr}\right)\left(S_{e[t]} - S_{e[w]}\right) \tag{2.33}$$

Once the LNAPL residual saturation distribution $S_{nr}(z)$ is known, equations (2.27), (2.28), and (2.33) may be used to calculate the vertical water and LNAPL saturation distributions.

2.4.4 "Initial" LNAPL Saturation Values and Residual LNAPL Saturation

LNAPL residual saturation may be estimated as a constant value based on soil texture and whether the location is in the saturated zone or vadose zone, or it may be estimated as a fraction of the local initial (maximum) LNAPL saturation, as suggested in Section 2.1.3. Furthermore, constant LNAPL residual saturation values may be estimated for different soil layers based on the maximum LNAPL saturation within each layer, and with different f-factor values for different soil layers. These capabilities are provided within the LNAPL Distribution and Recovery Model (see Volume 2). This subsection concerns estimation of the initial LNAPL saturation distribution when the initial monitoring well thickness b_n is known, and when the variable LNAPL residual saturation model of Section 2.1.3 is used.

If the monitoring well LNAPL-thickness equals its maximum value, then the LNAPL saturation at any elevation will also equal its maximum value. According to equation (2.2), for this condition, $S_{nr} = f_r S_{ni}$. For $z < z_{an}$, the LNAPL saturation is calculated from $S_n = 1 - S_w$. With equation (2.27) this gives

$$S_{ni} = 1 - S_{wr} - \left(1 - S_{wr} - f_r S_{ni}\right) S_{e[w]}$$

Thus for $z < z_{an}$, the initial LNAPL saturation distribution is given by

$$S_{ni}(z) = \frac{(1 - S_{wr})(1 - S_{e[w]}(z))}{1 - f_r S_{e[w]}(z)} \quad (2.34)$$

Above the elevation z_{an} all three phases are present. For $z > z_{an}$, equation (2.33) gives

$$S_{ni} = f_r S_{ni} + (1 - S_{wr} - f_r S_{ni})(S_{e[t]} - S_{e[w]})$$

This equation may be arranged to give the initial LNAPL saturation distribution as

$$S_{ni}(z) = \frac{(1 - S_{wr})(S_{e[t]}(z) - S_{e[w]}(z))}{1 - f_r (1 + S_{e[w]}(z) - S_{e[t]}(z))} \quad (2.35)$$

At elevation $z = z_{an}$, $S_{e[t]} = 1$ and equation (2.35) is the same as equation (2.34). With equations (2.34) and (2.35) [based on the maximum monitoring well LNAPL thickness $b_{n[\max]}$], the residual LNAPL saturation distribution is

$$S_{nr}(z) = f_r \, S_{ni}(z) \quad (2.36)$$

The LNAPL residual saturation distribution specified by equation (2.36) will correspond to the maximum LNAPL thickness.

2.4.5 LNAPL Capillary Rise

The LNAPL capillary rise, $z_{\max}$, is the highest elevation of free-LNAPL corresponding to a specified monitoring well LNAPL thickness. At this elevation, $S_n(z) = S_{nr}$. A look at equation (2.32) or (2.33) shows that this corresponds to the condition $S_{e[t]} = S_{e[w]}$. With equations (2.24) and (2.30) this gives

$$\alpha_{nw}(z_{\max} - z_{nw}) = \alpha_{an}(z_{\max} - z_{an})$$

This equation gives

$$z_{\max} = \frac{\alpha_{an} z_{an} - \alpha_{nw} z_{nw}}{\alpha_{an} - \alpha_{nw}} \quad (2.37)$$

Equation (2.37) may also be written

$$z_{\max} = z_{an} + \frac{(1 - \rho_r)(\sigma_{an}/\sigma_{nw})}{\rho_r - (1 - \rho_r)(\sigma_{an}/\sigma_{nw})} b_n \quad (2.38)$$

One of the interesting features of this equation is that the LNAPL capillary rise depends only on fluid properties and not on soil texture. This is an interesting feature because the height of the capillary fringe (water capillary rise) above the water table clearly depends on soil texture, being much larger for clay than sand soil. A second feature of interest is that as the ratio σ_{an}/σ_{nw} increases, the LNAPL capillary rise increases. The limiting condition is

$$\frac{\sigma_{an}}{\sigma_{nw}} \leq \frac{\rho_r}{1-\rho_r} \tag{2.39}$$

If the limit specified by equation (2.39) is exceeded, then the LNAPL capillary rise reaches the ground surface (infinity).

2.4.6 Calculation of LNAPL Saturation Distribution from Monitoring-Well LNAPL Thickness

Field monitoring of LNAPL plumes will often provide data on elevations of the air-LNAPL and LNAPL-water interfaces, z_{an} and z_{nw}, respectively. Given a historical monitoring record, the largest LNAPL thickness, $b_{n[\max]}$, is used to estimate the LNAPL residual saturation distribution. This data along with the LNAPL density gives the water-table elevation using equations (2.19) or (2.20). Thus it is assumed that b_n, z_{an}, z_{aw}, and z_{nw} are known, along with fluid properties and soil texture (vG-parameter) characteristics. With this data, the following algorithm can be used to calculate the LNAPL saturation distribution:

1. Use the maximum LNAPL thickness, $b_{n[\max]}$, to calculate the LNAPL capillary rise using equation (2.37) or (2.38).
2. Calculate the "initial" LNAPL saturation distribution using equations (2.34) and (2.35).
3. Calculate the residual LNAPL distribution using equation (2.36).
4. For any other monitoring well LNAPL thickness (b_n), use equations (2.27), (2.28), and (2.33) to calculate the water and LNAPL saturation distributions.

An example saturation distribution is shown in Figure 2.15. This figure shows the water and LNAPL distributions at an initial and at a later time. The soil profile consists of a fine-grain zone (FGZ) overlying a coarser-grain layer. The facies interface is located at a depth of 5.5 meters below ground surface and the groundwater table is located at a depth of 5.0 m.

Section 2.6 of Volume 2 presents an example application of LDRM for data from a field site. The application uses a step-wise variable 'initial' LNAPL-thickness and step-wise variable water pumping rate to estimate LNAPL recovery.

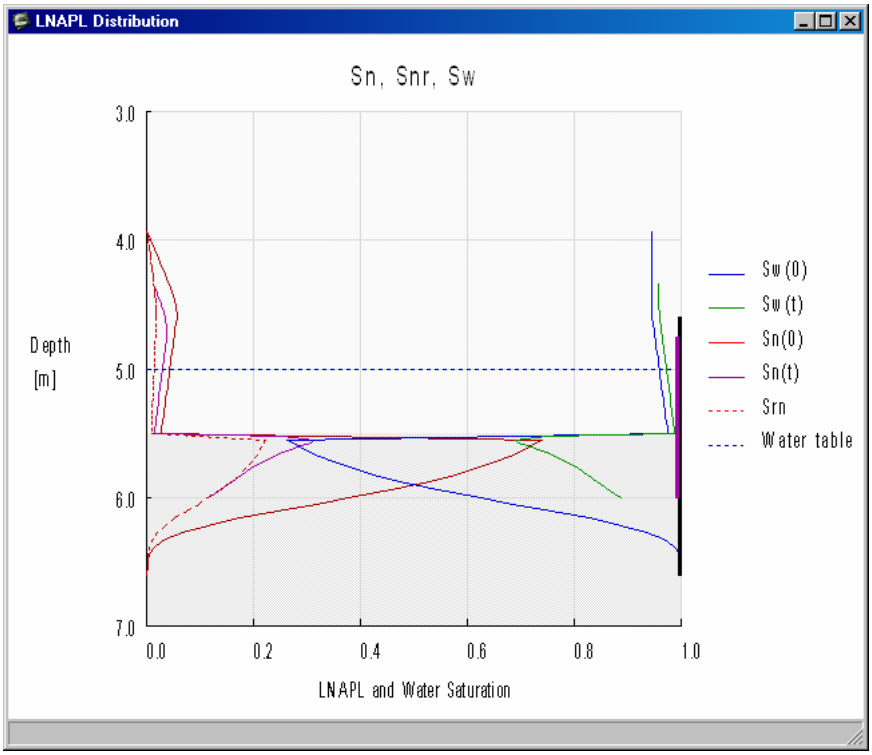

Figure 2.15—Calculated water and LNAPL saturation distributions based on two different LNAPL-thickness values

2.4.7 Free-LNAPL and Recoverable-LNAPL Specific Volume

Two quantities of great practical interest express the amount of free-LNAPL present in the formation and how much of this free-LNAPL is recoverable using hydrocarbon liquid recovery technologies. Under conditions of vertical equilibrium, both of these quantities can be related to the monitoring well thickness, b_n. LNAPL is considered "free" if it is present at a saturation exceeding residual. Both of these functions can be calculated directly from the LNAPL saturation and residual LNAPL saturation distributions.

The *LNAPL specific volume*, D_n, quantifies the amount of LNAPL present as a function of monitoring-well LNAPL thickness. It is determined by the area under the LNAPL saturation curve:

$$D_n(b_n) = \int_{z_{nw}}^{z_{max}} n\, S_n(z)\, dz \tag{2.40}$$

In equation (2.40), n is the porosity which may vary from one layer to another.

The *LNAPL recoverable volume*, R_n, is determined by the area between the LNAPL saturation curve and the residual saturation curve:

$$R_n(b_n) = \int_{z_{nw}}^{z_{max}} n\left(S_n(z) - S_{nr}(z)\right) dz \tag{2.41}$$

Both the LNAPL specific volume and recoverable volume curves are shown in Figure 2.16 for conditions shown in Figure 2.15. The LNAPL-transmissibility curve, which is discussed below, is also shown. The two dotted curves are piecewise linear approximations to the recoverable LNAPL and LNAPL-transmissibility curves. These approximation curves are also discussed below with regard to modeling of LNAPL recovery. With regard to the specific example shown in Figure 2.16, it is of interest to note that both the recoverable volume and transmissibility reach low values with more than 1 meter of LNAPL remaining in the monitoring well. This suggests that it will be difficult to achieve significant recovery with what appears to be a large LNAPL volume remaining in the formation based on the monitoring well thickness.

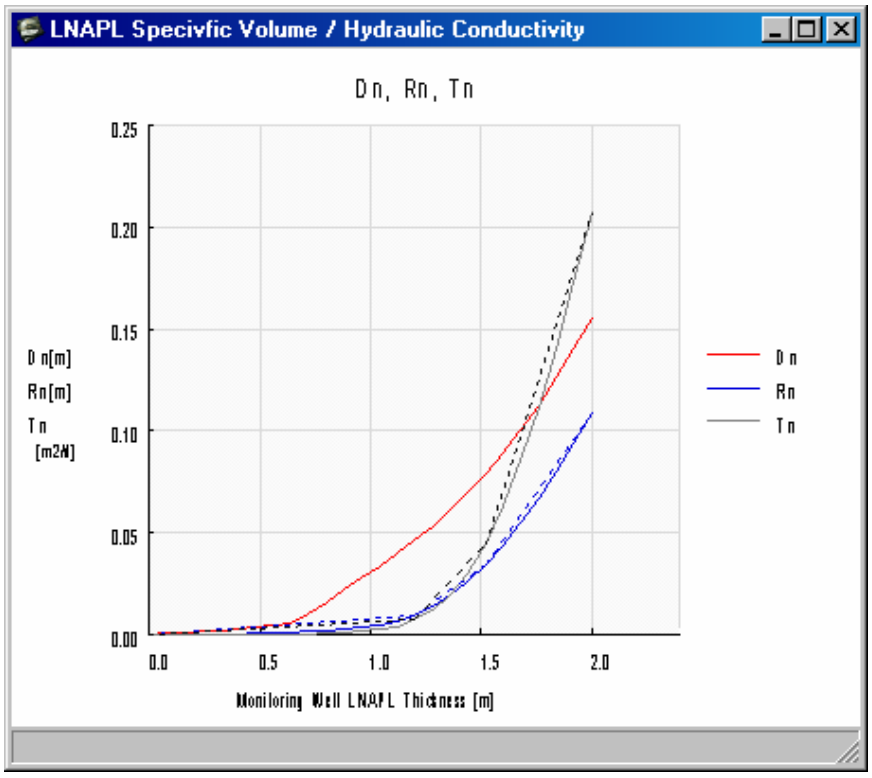

Figure 2.16—LNAPL specific volume and recoverable volume curves corresponding to Figure 2.15

3 LNAPL MOVEMENT

The purpose of this section is to describe the quantitative framework for estimating the possible movement of LNAPL within the subsurface environment. Relative permeability relationships are presented. Potential migration of LNAPL through fine-grain soils is discussed, as is the potential lateral migration of LNAPL into pristine soils. The primary focus of this section is development of the LNAPL-recovery rate equations for different LNAPL recovery technologies (single and dual pump wells, vacuum-enhanced wells, skimmer wells, and trenches). The case of potential recovery of LNAPL trapped beneath fine-grain soil using skimmer wells is also discussed.

3.1 LNAPL MOVEMENT AND DARCY'S LAW

3.1.1 Darcy's Law

Darcy's law may be used to quantify LNAPL flow. It may be written in the simple form

$$\vec{q}_n = K_n \vec{J}_n \tag{3.1}$$

In equation (3.1) q_n is the NAPL Darcy velocity (volume flux), K_n is the NAPL hydraulic conductivity, and J_n is the NAPL hydraulic gradient. K_n depends on NAPL and water saturation, as well as fluid and media properties. The saturation effect may be included by introducing the NAPL relative permeability, k_{rn}, which expresses the fraction of the NAPL saturated hydraulic conductivity that is effective at given saturation conditions. The NAPL saturated hydraulic conductivity is related to the water saturated hydraulic conductivity through

$$K_{ns} = K_{ws} \frac{\rho_r}{\mu_r} \tag{3.2}$$

In equation (3.2), ρ_r and μ_r are the NAPL/water density and viscosity ratio, respectively. The NAPL hydraulic gradient is calculated using equation (2.14). Together, these results allow Darcy's law to be written in the following convenient form

$$\vec{q}_n = \frac{K_{ws} k_{rn}(S_w, S_n)}{\mu_r} \left((1-\rho_r)\hat{k} - \frac{\nabla p_{c[nw]}}{\rho_w g} + \vec{J}_w \right) \tag{3.3}$$

With reference to the driving force for LNAPL flow given on the right side of equation (3.3), the first term is associated with buoyancy, the second term is associated with capillary pressure gradient and states that the LNAPL flow tends towards decreasing capillary pressure, and the third term is associated with the tendency of LNAPL to migrate in the direction of groundwater flow. In the case of heterogeneous soils, if one can associate decreasing capillary pressure with increasing pore size (the radius of curvature of the interface between LNAPL and water is larger in larger pores), it is the middle term that provides the tendency for LNAPL to accumulate within coarse-grain soil and makes it harder for LNAPL to migrate into fine-grain soil.

Beyond the driving forces causing LNAPL migration, equation (3.3) states that the flow (volume flux) is also dependent on the LNAPL relative permeability, which in turn depends on both the

water and LNAPL saturation. Development of this relationship between relative permeability and saturation for LNAPL is described below.

3.1.2 NAPL Relative Permeability: Burdine and Mualem Equations

While the NAPL relative permeability curve can be measured in the laboratory, this is seldom done because of experimental difficulties and cost. Instead, model equations are used to associate permeability with pore size, and then integrate over the range in pore sizes occupied by NAPL, and finally multiplying by a tortuosity coefficient. There are many different ways to do this. The two most commonly used models were developed by Burdine (1953) and Mualem (1976) [see van Genuchten, 1980; Parker et al., 1987; van Genuchten et al., 1991]. For the NAPL phase the Burdine equation is

$$k_{rn}\left(S_w, S_n\right) = \left(S_{e[t]} - S_{e[w]}\right)^2 \left(\frac{\int_{S_{e[w]}}^{S_{e[t]}} \frac{dS_e}{h_c^{\,2}}}{\int_0^1 \frac{dS_e}{h_c^{\,2}}} \right) \tag{3.4}$$

The Mualem equation is written

$$k_{rn}\left(S_w, S_n\right) = \sqrt{S_{e[t]} - S_{e[w]}} \left(\frac{\int_{S_{e[w]}}^{S_{e[t]}} \frac{dS_e}{h_c}}{\int_0^1 \frac{dS_e}{h_c}} \right)^2 \tag{3.5}$$

The basic form of both equations (3.4) and (3.5) is the same. The leading term on the right is a tortuosity factor, while the second term involving the integrals is a permeability-weighting of pore size occupied by NAPL (see equation 2.1 relating capillary pressure and radius). In particular, the Burdine equation assigns contributions to relative permeability based on the radius-squared, just as in the Hagan-Poiseuille equation for flow in a capillary tube.

In order to evaluate equations (3.4) and (3.5), equation (2.3) is inverted to give

$$h_c = \frac{1}{\alpha}\left(\frac{1 - S_e^{\,1/M}}{S_e^{\,1/M}} \right)^{1/N} \tag{3.6}$$

Consider first the Burdine equation. The integral in the numerator becomes

$$F_1\left(S_{e[w]}, S_{e[t]}\right) = \alpha^2 \int_{S_{e[w]}}^{S_{e[t]}} \left(S_e^{\,1/M}\right)^{2/N} \left(1 - S_e^{\,1/M}\right)^{-2/N} dS_e$$

Substitute $y = S_e^{1/M} \rightarrow dS_e = M\, y^{(M-1)}\, dy$, and $M = 1 - 2/N$, then this integral becomes

$$F_1\left(S_{e[w]}, S_{e[t]}\right) = \alpha^2 M \int_{S_{e[w]}^{1/M}}^{S_{e[t]}^{1/M}} (1-y)^{-2/N}\, dy = \alpha^2 \left\{ \left(1 - S_{e[w]}^{1/M}\right)^M - \left(1 - S_{e[t]}^{1/M}\right)^M \right\}$$

In particular, $F_1(0,1) = \alpha^2$. Thus the van Genuchten-Burdine (vG-B) relative permeability function becomes

$$k_{rn}\left(S_w, S_n\right) = \left(S_{e[t]} - S_{e[w]}\right)^2 \times \left(\left(1 - S_{e[w]}^{1/M}\right)^M - \left(1 - S_{e[t]}^{1/M}\right)^M \right) \tag{3.7}$$

Calculations for the Mualem equation are similar. With equation (3.6), the integral in the numerator becomes

$$F_2\left(S_{e[w]}, S_{e[t]}\right) = \alpha \int_{S_{e[w]}}^{S_{e[t]}} \left(S_e^{1/M}\right)^{1/N} \left(1 - S_e^{1/M}\right)^{-1/N} dS_e$$

Substitute $y = S_e^{1/M} \rightarrow dS_e = M\, y^{(M-1)}$ dy, and $M = 1 - 1/N$, then the integral becomes

$$F_2\left(S_{e[w]}, S_{e[t]}\right) = \alpha M \int_{S_{e[w]}^M}^{S_{e[t]}^M} (1-y)^{-1/N}\, dy = \alpha \left(\left(1 - S_{e[w]}^{1/M}\right)^M - \left(1 - S_{e[t]}^{1/M}\right)^M \right)$$

In particular, $F_2(0,1) = \alpha$. Thus the relative permeability for the Mualem model becomes

$$k_{rn}\left(S_w, S_n\right) = \sqrt{S_{e[t]} - S_{e[w]}} \times \left(\left(1 - S_{e[w]}^{1/M}\right)^M - \left(1 - S_{e[t]}^{1/M}\right)^M \right)^2 \tag{3.8}$$

Equations (3.7) and (3.8) show that the NAPL relative permeability value depends on both the water and NAPL saturation. This may be understood by considering Figure 2.10. Larger water saturation will cause the NAPL to reside in larger pore spaces having higher associated permeability.

An interesting application of equations (3.7) and (3.8) is for a two-phase system for which $S_{e[t]} = 1$ and $S_n = 1 - S_w$. For this condition the effective water saturation becomes $S_{e[w]} = \dfrac{1 - S_n - S_{wr}}{1 - S_{nr} - S_{wr}}$ and $1 - S_{e[w]} = \dfrac{S_n - S_{nr}}{1 - S_{nr} - S_{wr}}$. Equations (3.7) and (3.8) become

$$k_{rn}\left(S_n\right) = \left(1 - S_{e[w]}\right)^2 \left(1 - S_{e[w]}^{1/M}\right)^M \tag{3.9}$$

$$k_{rn}\left(S_n\right) = \sqrt{1 - S_{e[w]}} \left(1 - S_{e[w]}^{1/M}\right)^{2M} \tag{3.10}$$

When S_n has its smallest value ($S_n = S_{nr}$; $S_{e[w]} = 1$; $1–S_{e[w]} = 0$), it is clear that $k_{rn}(S_{nr}) = 0$. However, when S_n takes is largest value ($S_n = 1–S_{wr}$; $S_{e[w]} = 0$), these equations give $k_{rn}(1–S_{wr}) = 1$. This is not correct because residual water still occupies part of the pore space. The issue can be associated with the tortuosity term, for which theory is limited.

Looking for a conceptually consistent tortuosity model, it appears that use of effective saturation rather than saturation itself leads to part of the problem. Also, if one used $S_n–S_{nr}$ in the tortuosity term, then at maximum NAPL saturation, the tortuosity reduction would be associated with the value $1–S_{wr}–S_{nr}$; that is, the NAPL residual would contribute to the tortuosity reduction even though that fraction of the pore space is occupied by NAPL (perhaps this makes sense if one thinks of residual NAPL as NAPL that is always immobile, rather than NAPL that becomes trapped and immobile as the free NAPL is removed). Conceptually, it appears that the most consistent approach is to use S_n in the tortuosity term, so its value ranges from S_{nr} to $1–S_{wr}$. Thus the suggested relative permeability models for NAPL are

$$k_{rn}(S_n) = S_n^{\,2}\left(1 - S_{e[w]}^{\,1/M}\right)^M \tag{3.11}$$

$$k_{rn}(S_n) = \sqrt{S_n}\left(1 - S_{e[w]}^{\,1/M}\right)^{2M} \tag{3.12}$$

Similar changes are made to the tortuosity term for the three-phase equations, which become

$$k_{rn}(S_w, S_n) = (S_n)^2 \times \left(\left(1 - S_{e[w]}^{\,1/M}\right)^M - \left(1 - S_{e[t]}^{\,1/M}\right)^M\right) \tag{3.13}$$

$$k_{rn}(S_w, S_n) = \sqrt{S_n} \times \left(\left(1 - S_{e[w]}^{\,1/M}\right)^M - \left(1 - S_{e[t]}^{\,1/M}\right)^M\right)^2 \tag{3.14}$$

3.1.3 Comparison of Relative Permeability Models

Figure 3.1 shows the predicted two-phase relative permeability functions for the Burdine and Mualem models based on the parameters from Figure 2.8. Generally one finds that the Mualem model will predict a larger relative permeability than the Burdine model. There is little information to suggest which model should be used. However, experience does suggest that the Burdine model may be more appropriate for coarse-grain soils. For fine-grain materials the Mualem model must be used; because for fine grain soils, the Burdine equations would predict nearly zero relative permeability under conditions where it is known that LNAPL flows to a recovery well.

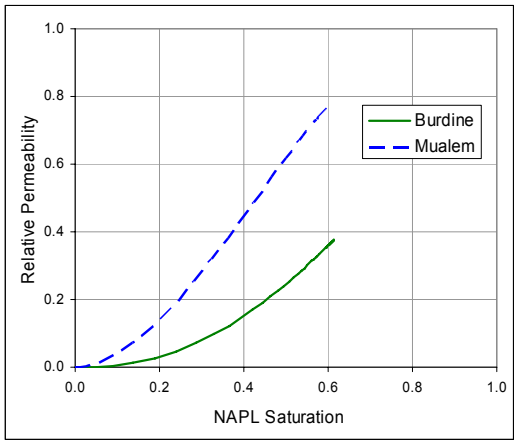

Figure 3.1—NAPL relative permeability predictions for the Burdine and Mualem models for parameters presented in Figure 2.8

3.2 LNAPL VERTICAL MIGRATION THROUGH FINE-GRAIN SOIL

LNAPL accumulations at considerable depths beneath the water table have been observed in the field. Often, such accumulations have resulted in LNAPL being trapped beneath fine-grain soils at locations with strong downward hydraulic gradients (Adamski, et al., 2005). This subsection discusses a potential mechanism for such LNAPL accumulations.

3.2.1 Effect of Vertical Gradients on LNAPL Saturation

Return to equation (3.3) and consider only the vertical component, which may be written

$$\frac{q_{nz}\mu_r}{K_{ws}k_{rn}} = (1-\rho_r) - \frac{1}{\rho_w g}\frac{dp_{c[nw]}}{dz} + J_{wz} \tag{3.15}$$

In fine-grain soils located near the ground surface, strong downward hydraulic gradients are commonly associated with groundwater recharge to an underlying permeable geologic unit. LNAPL vertical equilibrium (no LNAPL vertical flow) can still occur in the presence of downward water hydraulic gradient. If the downward hydraulic gradient does not exceed a critical value, then the capillary pressure distribution (with q_{nz} = 0) will satisfy the following equation (compare with equation 2.14):

$$p_{c[nw]} = \left((\rho_w - \rho_n)g + \rho_w g J_{wz}\right)(z - z_r) \tag{3.16}$$

In terms of the capillary pressure head (see equation 2.23) equation (3.16) may be written

$$h_{[nw]} = \left((1-\rho_r) + J_{wz}\right)(z - z_r) \tag{3.17}$$

Equation (2.24) may still be used to predict the effective saturation with a modified scaling factor to take into account the downward water hydraulic gradient in addition to interfacial tension and buoyancy effects:

$$\alpha_{nw}^{\ *} = \alpha_{nw}\left(1 + \frac{J_{wz}}{(1-\rho_r)}\right) \tag{3.18}$$

There is no change in the air-NAPL capillary pressure relationship, so equations (2.30) and (2.31) still hold.

As an example, Figure 3.2 shows the LNAPL distribution for a fine-grain soil with the following parameters: N = 1.5, α = 0.2 ft^{-1} (0.0066 cm^{-1}), S_{wr} = 0.35, S_{nrv} = 0.02, S_{nrs} = 0.05, ρ_r = 0.85. Two cases are shown, one for zero water hydraulic gradient, and the second for a water hydraulic gradient J_{wz} = -0.10. Both cases correspond to an 8-ft LNAPL thickness in a monitoring well (residual saturation distribution corresponds to an initial 10-ft LNAPL thickness). There is a significant decrease in resulting NAPL saturation associated with the downward water-phase hydraulic gradient.

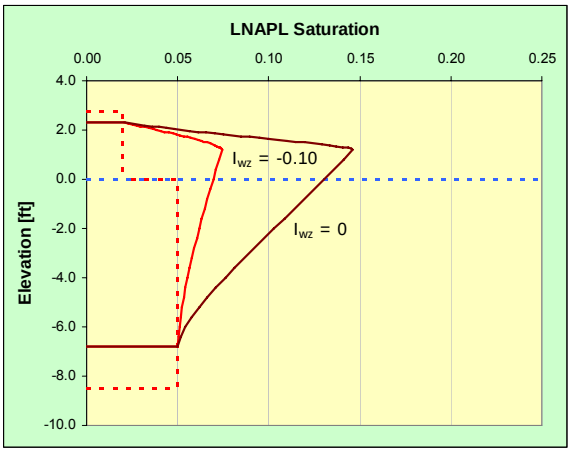

Figure 3.2—LNAPL distribution showing the effect of vertical hydraulic gradient

3.2.2 Critical Downward Hydraulic Gradient

If $J_{wz} < -(1 - \rho_r)$ then according to equation (3.17), the capillary pressure head would decrease with increasing elevation. This condition cannot exist; it would correspond to a NAPL saturation decreasing with elevation from an initial residual saturation value (see Figure 3.2). Thus the critical condition for downward displacement of LNAPL through fine-grain soil is

$$J_{wz} \le -(1-\rho_r) \tag{3.19}$$

In order for the downward gradient to exist, there must be a permeable zone at depth, and the displaced LNAPL would accumulate in this region.

3.3 LNAPL LATERAL MIGRATION AND LIQUID FREE-PRODUCT RECOVERY

This subsection discusses the lateral migration of LNAPL. First, issues associated with possible lateral migration of LNAPL into pristine soils (soils not directly impacted by the presence of LNAPL) are addressed, and it is noted that an LNAPL plume may retain appreciable LNAPL thickness in a monitoring well and yet be stable against lateral migration. Next, the vertical distribution of LNAPL mobility is described using the mobility ratio. It is shown that LNAPL has the greatest potential for movement within the upper parts of the capillary fringe. Finally,

lateral migration is quantified using the LNAPL transmissibility, with applications to LNAPL recovery using wells and trenches.

3.3.1 Lateral Migration of LNAPL into Pristine Soils

NAPL is the nonwetting phase with respect to water and the wetting phase with respect to air. In order to migrate laterally into regions not previously containing LNAPL, the LNAPL must displace either water or air from the pore space near the water table. In order to displace water, it must overcome the displacement pressure head between NAPL and water.

For NAPL migration into a water-saturated rock, the displacement pressure has been estimated by Hubbert (1953) as

$$p_c = \frac{C\sigma\cos(\theta_c)}{d} \tag{3.20}$$

In this equation, d is the mean grain diameter. Hubbert (1953) gives order of magnitude estimates $\sigma\cos(\theta_c) = 25$ dynes/cm and $C = 16$. For a silt (d = 1/256 to 1/16 mm) or sand (d = 1/16 to 2 mm), p_c ranges from 1 to 1/16 atm (101.3 kPa to 6.3 kPa) and 1/16 to 1/500 atm (6.3 kPa to 200 Pa), respectively. For example, using equation (2.16), a capillary pressure of 5 kPa would be achieved at an elevation 2.5 m above the reference point (LNAPL-water interface in a monitoring well).

However, such large LNAPL thickness need not be achieved for lateral spreading of LNAPL along the water table. If the LNAPL thickness exceeds a critical value, LNAPL will readily move into pore space occupied by air as the wetting fluid. A question of interest is how to calculate the LNAPL head required for spreading.

Selection of Models

The van Genuchten (vG) model has found wide use because it provides a smooth function in predicting the vertical saturation distribution and may readily be fit to both laboratory and field data. The smoothness of the function, remaining continuous throughout the range of fluid pressures, is an important attribute in numerical modeling of NAPL flow. With the vG model, for any positive LNAPL head (LNAPL head and monitoring well thickness are related through equation 2.22), part of the porous medium will have a LNAPL saturation exceeding LNAPL residual saturation, and will have a finite (non-zero) relative permeability (using either the Burdine or Mualem models). The vG model predicts that as long as $h_n > 0$, the LNAPL phase has the potential for movement. These characteristics are reasonable for predicting LNAPL recovery. As long as the LNAPL head (or b_n) is greater than zero, LNAPL should be free to migrate to a recovery well or trench as a separate-phase liquid. Thus, use of the vG capillary pressure model for simulating LNAPL recovery from previously impacted soils appears to be appropriate. However, the ability to model potential lateral migration into pristine soil is more uncertain. There is nothing within this modeling framework to suggest that this might not happen, and this is contrary to the fact that a positive capillary pressure is required for a non-wetting phase (LNAPL) to displace a wetting phase (water) from pore space. A model with a defined displacement pressure head is more appropriate for addressing issues associated with lateral spreading of LNAPL plumes.

The capillary pressure curve model presented by Brooks and Corey (1964) has a well-defined displacement pressure head. In addition to having a simpler form than the vG model, the Brooks and Corey (BC) model may adequately fit laboratory and field data in many cases. The BC model predicts a limit to lateral spreading of an LNAPL plume following source control. Such features have been incorporated in EPA's Hydrocarbon Spill Screening Model (HSSM) (Weaver et al., 1994; Charbeneau et al., 1995). The BC model also predicts that LNAPL recovery would cease while a finite LNAPL head (or b_n) still exists in monitoring wells. This unrealistic expectation led to change from the BC model in earlier versions of the LNAPL recovery model to the present use of the vG capillary pressure model. In this regard, it appears that the vG and BC models have attributes for different applications. Application of the BC model is described in the following paragraphs.

The Brooks and Corey (1964) power-law model takes the form

$$S_e = \left(\frac{h_d}{h_c} \right)^{\lambda} \quad ; \quad h_c \geq h_d$$
$$S_e = 1 \quad ; \quad h_c < h_d \tag{3.21}$$

In equation (3.21), h_d is the displacement pressure head and λ is the BC pore size distribution parameter. These are the two BC parameters, corresponding to the vG parameters α and N.

Figure 3.3 compares the vG and BC capillary pressure models fit to measured soil capillary pressure data. The fitted parameters for the BC model are h_d = 1.01 m, λ = 0.79, and S_{wr} = 0.24. As judged based on the root-mean-square error (RMSE), this model provides the best fit to the data. The fit for both versions of the vG model is similar, with the vG-Burdine model having a smaller RMSE. The estimated vG-B parameters are N = 3.75 (M = 0.47), α = 0.67 m^{-1}, and S_{wr} = 0.36. The BC model predicts a well-defined capillary fringe of height about 100 cm. Above this height the capillary pressure is large enough for air to be present within the larger pore spaces, and the water saturation decreases. The BC model is considered appropriate for analysis of potential lateral migration of LNAPL into regions previously unexposed.

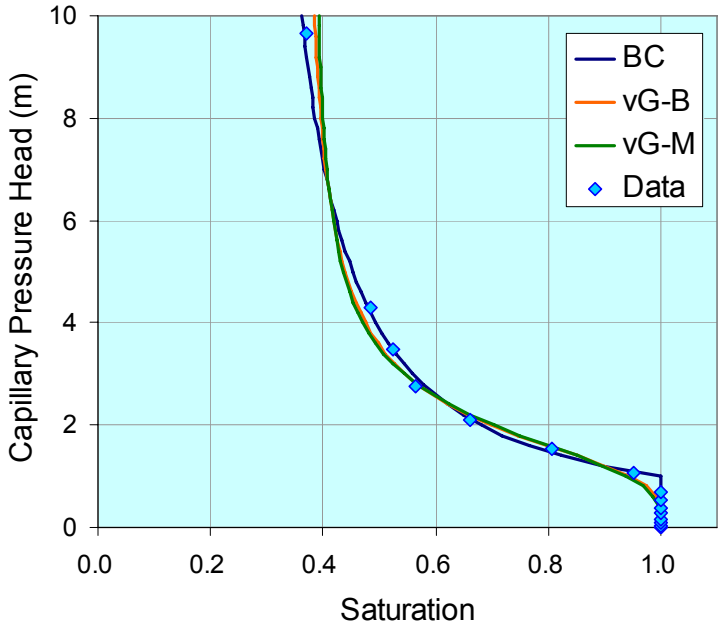

Figure 3.3—Water saturation curves predicted by the vG and BC models

Lateral migration of LNAPL requires that movement of LNAPL from a fluid system with capillary pressure distribution shown in Figure 2.14 into a region with capillary pressure distribution shown in Figure 2.13. The LNAPL must displace either water or air from the pore space. However, there is a significant difference in these two possibilities. LNAPL displaces water as the nonwetting fluid, and thus a positive capillary pressure is required to force the wetting fluid from the pore space. On the other hand, LNAPL displaces air as the wetting fluid, and the resulting capillary pressure gradient will pull the LNAPL into the air-filled pore space. This is the reason for LNAPL capillary rise above the water table.

Capillary pressure models with an explicit displacement pressure head, such as equation (3.21), allow one to calculate the necessary monitoring well thickness for lateral migration of LNAPL along the water table. The same methods described in Section 2 can be used to predict the LNAPL saturation distribution. The air-water displacement head is scaled analogously to the vG-α. The equations analogous to equations (2.25) and (2.31) are

$$h_{d[nw]} = \frac{\sigma_{nw}}{(1-\rho_r)\sigma_{aw}} h_d \tag{3.22}$$

$$h_{d[an]} = \frac{\sigma_{an}}{\rho_r \sigma_{aw}} h_d \tag{3.23}$$

If the LNAPL-water capillary pressure head exceeds $\sigma_{nw} h_d/\sigma_{aw}$ (see equation 2.9), then LNAPL can enter the porous media displacing water. Under conditions of vertical equilibrium, this will occur at an elevation given by equation (2.23). Thus the head $h_{d[nw]}$ specified in equation (3.22) corresponds to the elevation above the LNAPL-water interface in a monitoring well at which LNAPL can displace water, entering the porous medium. Similarly, the head $h_{d[an]}$ corresponds to the elevation above the air-LNAPL interface in a monitoring well at which air can displace 'total

liquid' (water plus LNAPL). Considering Figure 2.14, LNAPL can displace water from the porous media at an elevation $h_{d[nw]}$ above the LNAPL-water interface, z_{nw}. Below this elevation there is not sufficient capillary pressure. Similarly, air would not be present below an elevation $h_{d[an]}$ above the air-LNAPL interface, z_{an} (or an elevation h_d above the water table z_{aw} if no LNAPL is present). Thus, unless the elevations z_{an} and z_{nw} are far enough apart, there is no ability for the LNAPL to penetrate the medium. Thus the limiting condition for LNAPL lateral migration is

$$z_{an} + h_{d[an]} \geq z_{nw} + h_{d[nw]} \tag{3.24}$$

Since $b_n = z_{an} - z_{nw}$, equation (3.24) gives (Charbeneau, et al., 1999)

$$b_{n[crit]} = \left(\frac{\sigma_{nw}}{(1-\rho_r)\sigma_{aw}} - \frac{\sigma_{an}}{\rho_r \sigma_{aw}} \right) h_d \tag{3.25}$$

Figure 3.4 illustrates the concepts presented in the previous paragraph. The soil parameters correspond to Figure 3.3 (with h_d = 1.0 m) and fluid properties ρ_r = 0.8, σ_{aw} = 65 dyne/cm, σ_{an} = 25 dyne/cm, and σ_{nw} = 20 dyne/cm. The critical LNAPL thickness corresponding to equation (3.25) is $b_{n[\text{crit}]}$ = 1.06 m, and the example shown has b_n = 1.2 m. To the right side of the figure is shown the LNAPL thickness (b_n), the displacement pressure heads ($h_{d[nw]}$ and $h_{d[an]}$), and the LNAPL head (h_n) calculated from equation (2.22). The water table is taken as the datum. One may distinguish a number of different regions. Between the elevation z_{nw} and $z_{nw}+h_{d[nw]}$, the capillary pressure head between LNAPL and water is increasing but remains below $\sigma_{nw}\, h_d/\sigma_{aw}$, so that only water can occupy the pore space according to the BC model. The second region occurs between elevations $z_{nw}+h_{d[nw]}$ and $z_{an}+h_{d[an]}$. In this region the capillary pressure head between LNAPL and water exceeds $\sigma_{nw}\, h_d/\sigma_{aw}$, so that LNAPL can penetrate the larger pores displacing the water. However, the capillary pressure head between air and LNAPL is less than $\sigma_{an}\, h_d/\sigma_{aw}$, so that air is unable to displace liquids (water plus LNAPL from the porous media). The effective water saturation (defined in equation 2.26) is shown as the blue curve near the upper right corner of the figure. The third region extends from elevation $z_{an}+h_{d[an]}$ to elevation $z_{\max}$. Within this region the LNAPL-water capillary pressure exceeds $\sigma_{nw}\, h_d/\sigma_{aw}$ while the air-LNAPL capillary pressure exceeds $\sigma_{an}\, h_d/\sigma_{aw}$, so that LNAPL can displace water from the pore space and air can displace 'total liquid'. The red curve near the upper right corner of the figure shows the effective total liquid saturation (defined in equation 2.32). The air-LNAPL capillary pressure increases at a larger rate with elevation (see Figure 2.14), and the effective water and effective total liquid curves come together at the elevation $z_{\max}$ (with the parameters for this example, $z_{\max}$ = 0.745 m). At elevation $z_{\max}$, $S_{e[w]} = S_{e[t]}$, and the LNAPL saturation is equal to its residual value. Equation (2.38) still applies for the elevation of LNAPL capillary rise. The LNAPL saturation shown as the solid curve on the left of the figure is calculated using equation (2.33), where for simplicity it is assumed S_{nr} = 0. For comparison, the LNAPL saturation distribution calculated using the van Genuchten model is also shown. It is clear that the van Genuchten model predicts a much larger vertical extent with LNAPL saturation greater than residual, and a correspondingly larger LNAPL specific volume.

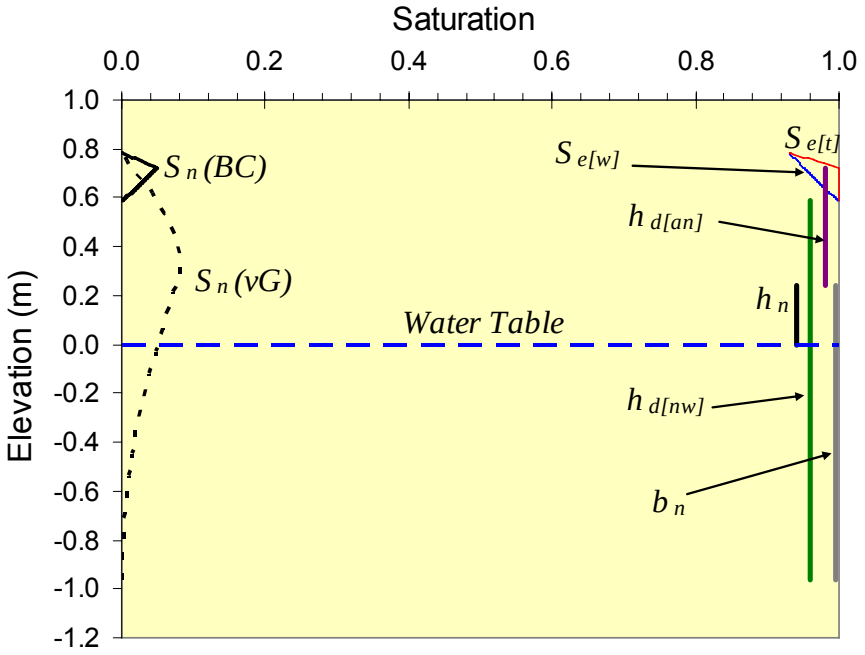

Figure 3.4—LNAPL saturation distribution predicted using the Brooks and Corey capillary pressure model with $b_n > b_{n[crit]}$

The limiting case with $b_n = b_{n[crit]}$ is shown in Figure 3.5. For this case there is still a significant LNAPL saturation predicted using the van Genuchten model but no LNAPL saturation predicted using the Brooks and Corey model. Substituting equation (3.25) into equation (2.38) shows that for this case, $z_{max} = z_{an} + h_{d[an]}$. The most significant point to this discussion is that with a capillary curve model such as that of Brooks and Corey that has a well defined displacement pressure head, LNAPL is not free to migrate laterally across the water table. There must be sufficient head (LNAPL thickness) to cause movement of LNAPL into regions not previously impacted. Migration of free liquid LNAPL is generally limited in the environment.

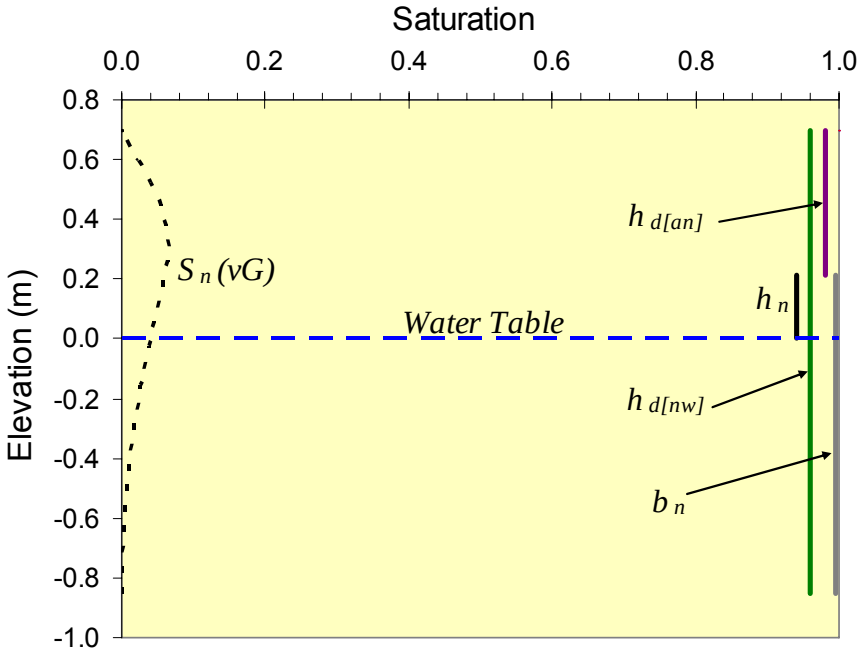

Figure 3.5—Limiting LNAPL saturation distribution (none) predicted using the Brooks and Corey capillary pressure model with $b_n = b_{n[crit]}$

3.3.2 LNAPL Mobility Ratio

Equation (3.3) can be used to predict the lateral migration of LNAPL towards a trench or recovery well. For horizontal flow in the x-direction this may be written

$$q_{nx} = \frac{K_{ws} k_{rn}}{\mu_r} \left(\frac{-1}{\rho_w g} \frac{dp_{c[nw]}}{dx} + J_{wx} \right) \tag{3.26}$$

Vertical variations in $p_{c[nw]}$ determine the vertical NAPL saturation distribution. If the LNAPL saturated thickness remains uniform (b_n does not change laterally), then the lateral gradient in capillary pressure will vanish, and equation (3.26) takes the very simple form

$$q_{nx} = \frac{K_{ws} k_{rn} J_{wx}}{\mu_r} = \frac{k_{rn} q_{wx}}{k_{rw} \mu_r} \tag{3.27}$$

The ratio k_{rn}/μ_n is called the NAPL mobility while k_{rw}/μ_w is the water mobility (Bear, 1972). Thus equation (3.27) can be written in terms of the NAPL/water mobility ratio, $m_{r[nw]}$:

$$q_{nx} = m_{r[nw]} q_{wx} \tag{3.28}$$

It is of interest to investigate the vertical distribution in mobility ratio across the LNAPL layer. This requires the wetting phase (water) relative permeability function.

For the vG-Mualem model, the water relative permeability function is calculated using equation (3.5) with the limits changed to 0 → $S_{e[w]}$ in the integral of the numerator. This gives

$$k_{rw}(S_w) = \sqrt{S_w}\left(1-\left(1-S_{e[w]}^{1/M}\right)^M\right)^2 \tag{3.29}$$

Using equations (3.29) and (3.12), the mobility ratio becomes

$$\mu_r m_{r[nw]} = \sqrt{\frac{S_n}{S_w}}\left(\left(1-S_{e[w]}^{1/M}\right)^{-M}-1\right)^{-2} \tag{3.30}$$

When combined with equation (2.33), the vertical distribution of mobility ratio can be calculated.

An example plot of the mobility ratio is shown in Figure 3.6 This figure actually plots the ratio k_{rn}/k_{rw} as the mobility ratio. Significantly, the mobility of LNAPL far exceeds that of water in the upper part of the capillary fringe. The strong implication is that lateral flow in an LNAPL lens is not uniform. A computationally efficient model for calculating lateral LNAPL flow does not directly take into account this vertical variation. Instead, the model is based on the integrated mobility of the entire LNAPL layer thickness, as represented through the LNAPL transmissibility, which is presented in the next subsection.

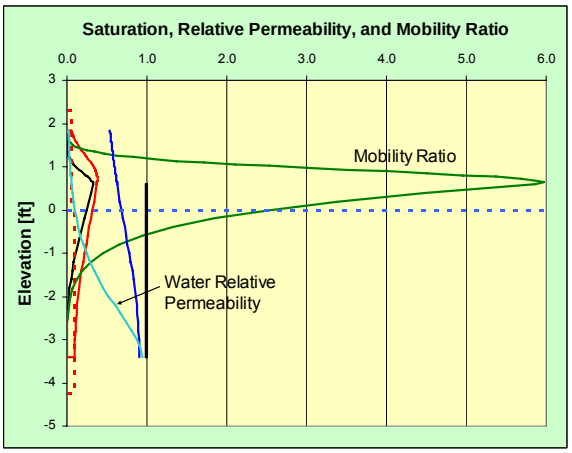

Figure 3.6—LNAPL/water mobility ratio

3.3.3 LNAPL—Layer Volume Flux

Assuming that the horizontal hydraulic gradient is uniform over depth near the water table, the horizontal volume flux for the LNAPL layer may be calculated by integrating the LNAPL specific discharge over the mobile thickness of the layer.

This calculation may be made by defining the LNAPL-layer transmissibility as follows:

$$T_n(b_n) = \frac{\rho_r}{\mu_r} \int_{z_{nw}}^{z_{max}} K_{ws}(z) k_{rn}(S_w, S_n)\, dz \tag{3.31}$$

In terms of the transmissibility, the lens unit flux (in the x-direction) is calculated from

$$U_{nx} = \int_{z_{nw}}^{z_{max}} q_{nx} dz = T_n(b_n)\, J_{nx} = \frac{T_n(b_n) J_{wx}}{\rho_r} \tag{3.32}$$

Equation (3.32) may be used to develop an important relationship between total LNAPL and water volume flux past a vertical surface (trench wall or screened section of a recovery well). If the vertical extent of water flow, b_w, extends below the LNAPL layer to an appreciable extent, then the water unit flux is $U_{wx} = T_w(b_w)\, J_{wx}$, and equation (3.32) may be written

$$U_{nx} = \frac{T_n(b_n)}{\rho_r T_w(b_w)} U_{wx} \tag{3.33}$$

In equation (3.33), the aquifer transmissivity (for water) is written as a function of the vertical depth b_w beneath the water table in order to represent that the transmissivity will depend on the elevation of the water table, the depth of penetration, and on the vertical distribution of hydraulic conductivity. This is not meant to imply that b_w changes with time (unlike b_n, which does). Equation (3.33) is an important result which leads to relationships for estimation of LNAPL-recovery system performance.

Another Approach for Flow to a Well

Equation (3.33) is very important in development of mathematical models for LNAPL recovery. In this subsection it is developed again from the point of view of flow towards a well.

When groundwater is produced from a pumping well, it creates a gradient that causes LNAPL migration towards the well. Larger groundwater pumping rates correspond to larger hydraulic gradients toward the well, and increased LNAPL flow. This is shown schematically in Figure 3.7. Groundwater pumping at a discharge Q_w over a screened interval b_w causes LNAPL to flow to the well at a rate Q_n, corresponding to monitoring well LNAPL thickness b_n. The LNAPL-layer transmissibility is defined by equation (3.31), and the water-layer transmissivity is defined by $T_w(b_w) = \int_{z_{aw}-b_w}^{z_{aw}} K_{ws}(z) dz$.

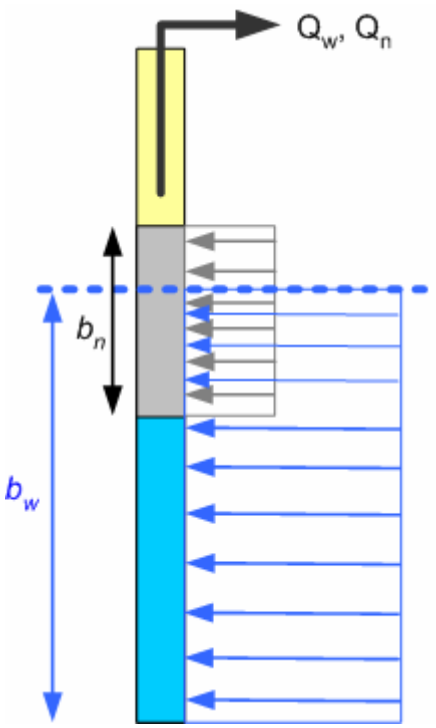

Figure 3.7—LNAPL and groundwater flow to a well

For small pumping rates, the flow towards the well is primarily horizontal, and the Thiem equation (Charbeneau, 2000) can be used to predict drawdown (s) and discharge. For each phase-j, the Thiem equation is written ($j = w, n$)

$$s_j = \frac{Q_j}{2\pi T_j} \ln\left(\frac{R_j}{R_W}\right) \tag{3.34}$$

Within equation (3.34), R_j is the radius of influence (R_I) for the water phase and the radius of capture (R_C) for the NAPL phase, and R_W is the well radius. Since groundwater production creates the gradient for production of both LNAPL and water, the radial pressure gradient is the same for both fluids (this is consistent with a constant capillary pressure):

$$\frac{s_w}{\ln\left(R_I / R_W\right)} = \frac{\rho_r s_n}{\ln\left(R_C / R_W\right)} \tag{3.35}$$

Equation (3.35) is consistent with equation (2.16) and is the same as

$$\frac{p_{wI} - p_{wW}}{\ln\left(R_I / R_W\right)} = \frac{p_{nC} - p_{nW}}{\ln\left(R_C / R_W\right)} \tag{3.36}$$

This is also consistent with writing the Thiem equation in the form (see Muskat, 1946, pg. 153).

$$Q = \frac{2\pi k b\left(p_e - p_w\right)}{\mu \ln\left(r_e / r_w\right)}$$

In this equation, k is the intrinsic permeability, b is the aquifer thickness, p_e is the external pressure at radius r_e from a well, p_w is the well pressure at radius r_w, and μ is the fluid dynamic viscosity. Together, equations (3.34) and (3.35) imply

$$\frac{Q_w}{T_w(b_w)} = \frac{\rho_r Q_n}{T_n(b_n)} \tag{3.37}$$

Equation (3.37) is the same as equation (3.33).

3.3.4 Vacuum-Enhanced Recovery

If a small vacuum is applied to a recovery well, air will be pulled into the well and the resulting pressure gradient will be transmitted to the LNAPL, causing it to also move into the well. Analysis of air flow is somewhat different than flow of water or NAPL because as the air pressure changes, the air density will change as well (according to the ideal gas law). For isothermal conditions, the pressure and density are related through

$$p_a = \rho_a \frac{p_{ao}}{\rho_{ao}} \tag{3.38}$$

In equation (3.38), p_a is the absolute pressure and p_{ao} and ρ_{ao} are the pressure and density at some reference or standard state.

For a vacuum-enhanced recovery system the source of the air is the atmosphere. Air movement is downward through the shallow vadose zone (leakage) and then laterally to the well. The flow situation is similar to flow of water to a well with recharge supplied through leakage from an adjacent aquifer across an aquitard. This is shown schematically in Figure 3.8.

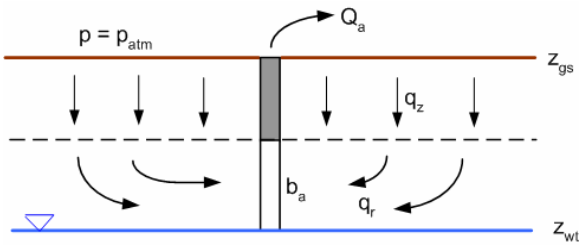

Figure 3.8—Air flow to a vacuum-enhanced recovery well with leakage from the atmosphere across the shallow vadose zone

For steady radial flow to a well over a screened interval b_a, the mass flux and mass rate of flow are calculated using Darcy's law:

$$f_{ar} = \rho_a q_{ar} = \rho_a \left(-\frac{k\bar{k}_{ra}}{\mu_a} \frac{dp_a}{dr} \right) \tag{3.39}$$

$$\dot{m}_{ar} = A_r f_{ar} = (2\pi r b_a)\rho_a \left(-\frac{k\bar{k}_{ra}}{\mu_a} \frac{dp_a}{dr} \right) = \frac{\pi b_a k \bar{k}_{ra} \rho_{ao}}{p_{ao}\mu_a} \left(-r \frac{dp_a^{\,2}}{dr} \right) \tag{3.40}$$

In equations (3.39) and (3.40) k is the intrinsic permeability and $\bar{k}_{ra}$ is the average relative permeability for air flow that is less than 1 because of residual water saturation. A value $\bar{k}_{ra}$ = 0.9 is assumed. The change in radial mass rate of flow is equal to the mass flux from the atmosphere. The steady-state continuity equation gives

$$\frac{1}{2\pi r}\frac{d\dot{m}_{ar}}{dr} + f_{az} = 0 \tag{3.41}$$

In equation (3.41) f_{az} is the vertical mass flux and is considered positive if there is flow out of the "aquifer" region. Because of the vacuum applied to the well, there is a mass flux into the aquifer region from the atmosphere. At any radial distance r from the well, the mass flux depends on the local air pressure and is calculated as shown in equation (3.42).

$$f_{az} = \rho_a\left(-\frac{k_z\bar{k}_{ra}}{\mu_a}\frac{dp_a}{dz}\right) = -\frac{k_z\bar{k}_{ra}\rho_{ao}}{2\mu_a p_{ao}}\frac{dp_a{}^2}{dz} = \frac{k_z\bar{k}_{ra}\rho_{ao}}{2\mu_a p_{ao}}\frac{\left(p_a{}^2 - p_{atm}{}^2\right)}{b_a{}'} \tag{3.42}$$

The notation k_z is introduced to differentiate the intrinsic permeability in the vertical direction from that in the horizontal (radial) direction, which has been designated k. In equation (3.42) $b_a{}' = z_{gs} - z_{wt} - b_a$. This is the depth of primarily vertical flow downward from the ground surface (see Figure 3.8), and it should be clear that z_{gs} and z_{wt} are elevations while b_a is the screen length of the well. Because of the applied vacuum, $p_a < p_{atm}$, and the mass flux given by equation (3.42) is negative. Substituting equations (3.40) and (3.42) into equation (3.41), the continuity equation for air flow to the well may be written

$$\frac{1}{r}\frac{d}{dr}\left(r\frac{dp_a{}^2}{dr}\right) - \frac{k_z}{kb_a b_a{}'}\left(p_a{}^2 - p_{atm}{}^2\right) = 0 \tag{3.43}$$

Equation (3.43) is known as a modified Bessel differential equation of order zero. In this case the unknown function is $p_a{}^2$. Far from the well the pressure is atmospheric. At the well (radius $r = R_W$) the boundary condition is

$$\dot{m}_{arW} = \frac{\pi b_a k\bar{k}_{ra}\rho_{ao}}{p_{ao}\mu_a}\left(-r\frac{dp_a{}^2}{dr}\right)\Bigg|_{R_W\to 0} = -\rho_{aW}Q_{aW} \tag{3.44}$$

In equation (3.44) ρ_{aW} and Q_{aW} are the air density and discharge at the well. The solution to equation (3.43) with (3.44) is

$$p_a{}^2 = p_{atm}{}^2 - \frac{Q_{aW}\mu_a p_{aW}}{\pi b_a k\bar{k}_{ra}}K_0\left(\frac{r}{B}\right) \tag{3.45}$$

In equation (3.45) K_0 is the modified Bessel function of the second kind of order zero, and the new parameter B is defined by

$$B = \sqrt{\frac{kb_a b_a{}'}{k_z}} \tag{3.46}$$

Equation (3.45) may be used to estimate the approximate radius of influence of a vacuum-enhanced recovery well. The procedure is to take an equation that accurately describes the pressure distribution near the well and extrapolate out to a radius at which the pressure equals atmospheric pressure. For small arguments the Bessel function is approximated as

$$K_0(r/B) \approx -\left(\ln\left(\frac{1}{2}\frac{r}{B}\right)+\gamma\right) = \ln\left(\frac{2B}{e^{\gamma} r}\right) \tag{3.47}$$

In this result γ is the Euler constant (γ = 0.5772…). With the logarithmic approximation and equation (3.45) the pressure equals atmospheric at a radius where the argument of the logarithm equals 1. This gives for the approximate radius of influence R_{aI}

$$r = R_{aI} = \frac{2B}{e^{\gamma}} = 1.123B \tag{3.48}$$

Thus the approximate *radius of influence* is given by

$$R_{aI} = 1.123\sqrt{\frac{kb_a\left(z_{gs} - z_{wt} - b_a\right)}{k_z}} \tag{3.49}$$

The solution given by equation (3.45) can be used to calculate the air discharge from the well for an applied vacuum pressure. The equation directly gives the discharge at the well corresponding to the vacuum (well) pressure. The discharge corresponding to standard conditions is calculated using $Q_{ao} = Q_{aW}\ (\rho_{aW}/\rho_{ao})$. This leads to the following result (for the well radius the approximation given by equation (3.47) is excellent):

$$Q_{ao} = \frac{\pi b_a k \bar{k}_{ra}}{p_{ao}\mu_a}\left(\frac{{p_{atm}}^2 - {p_{aW}}^2}{\ln\left(R_{aI}/R_W\right)}\right) \tag{3.50}$$

However, the suction is usually small compared with atmospheric pressure, and the following approximate relationship holds:

$$\frac{{p_{atm}}^2 - {p_{aW}}^2}{p_{ao}} = \frac{\left(p_{atm} + p_{aW}\right)}{p_{ao}}\left(p_{atm} - p_{aW}\right) \cong 2\left(p_{atm} - p_{aW}\right) \tag{3.51}$$

One finally has the expression for the well air discharge as follows.

$$Q_{ao} = \frac{2\pi b_a k \bar{k}_{ra}}{\mu_a}\left(\frac{p_{atm} - p_{aW}}{\ln\left(R_{aI}/R_W\right)}\right) = \frac{2\pi T_w\left(b_a\right)\bar{k}_{ra}}{\mu_{ar}}\left(\frac{s_{aW}}{\ln\left(R_{aI}/R_w\right)}\right) \tag{3.52}$$

In equation (3.52) $T_w(b_a)$ is the transmissivity (for water) of the formation over the screened interval of the vadose zone (b_a), μ_{ar} is the air-water viscosity ratio (assumed to be μ_{ar} = 0.018), and s_{aW} is the suction drawdown measured in "water head – feet or meters". The later form of equation (3.52) is convenient because it can be calculated directly using hydraulic conductivity data for the formation.

LNAPL located near the water table is exposed to the air pressure gradient created by the applied vacuum pressure at the well. This air pressure gradient causes a head gradient within the LNAPL, causing it to move towards the recovery well (see equation 2.17). Equating the pressure gradients for the LNAPL and air phases, the following relationship results (see equation 3.52 and Section 3.3.3):

$$Q_n = \frac{\mu_{ar} T_n(b_n) Q_{ao}}{\rho_r \bar{k}_{ra} T_w(b_a)} = 2\pi T_n(b_n)\left(\frac{s_{aW}/\rho_r}{\ln(R_{aI}/R_W)}\right) \tag{3.53}$$

3.3.5 LNAPL Recovery Using Skimmer Wells

A skimmer well will recover LNAPL that enters the well with essentially no production of groundwater. It generally has a small radius of capture and limited LNAPL recovery rate because drawdown is limited to that which can develop within the LNAPL layer itself. Figure 3.9 shows a schematic view of LNAPL flowing towards a recovery well, where the LNAPL thickness at the radius of capture is b_n, and there is no thickness at the well (maximum recovery rate).

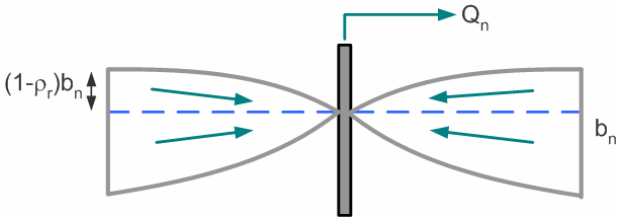

Figure 3.9—LNAPL recovery using a skimmer well

The LNAPL head at the radius of capture, R_C, is $h_n = (1-\rho_r)b_n$ (see equation 2.22), while the average LNAPL layer thickness is $b_n/2$. Using these values in the Thiem equation written for the LNAPL layer gives

$$Q_n = 2\pi K_{ns} \bar{k}_{rn} (b_n/2) \frac{((1-\rho_r)b_n - 0)}{\ln(R_C/R_W)} \tag{3.54}$$

This equation may be written

$$Q_n = \frac{\pi(1-\rho_r) T_n(b_n) b_n}{\ln(R_C/R_W)} \tag{3.55}$$

In equation (3.55) $T_n(b_n)$ is the LNAPL layer transmissibility. Equation (3.55) is analogous to applying the Dupuit model (see Charbeneau, 2000) for the LNAPL layer, and the form of the equation was developed by Johns et al. (2003) using different methods.

3.3.6 Recovery of LNAPL from Beneath Fine-Grain Zones Using Skimmer Wells

The procedure used to develop the skimmer well recovery equation in the previous Section is also used in development of a performance equation for a well skimming LNAPL trapped beneath a fine-grain zone (FGZ). However, both the form of the driving head and the average LNAPL thickness must be modified. The configuration is shown schematically in Figure 3.10.

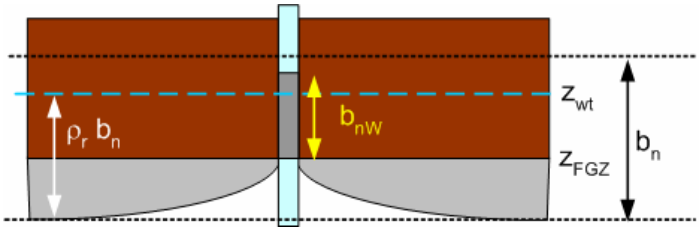

Figure 3.10—LNAPL trapped beneath FGZ and skimmer-well recovery

The LNAPL head for fluid entering the well corresponds to a monitoring well thickness determined by the elevation difference between the water table and the FGZ. The limiting LNAPL head at the well that can be sensed by LNAPL beneath the FGZ has $z_{nw} = z_{FGZ}$. The corresponding LNAPL thickness in the well is shown as b_{nW} in Figure 3.10, and the corresponding relationship is (see equation 2.20, where $z_{wt} = z_{aw}$)

$$b_{nW} = \left(z_{wt} - z_{FGZ}\right)/\rho_r \tag{3.56}$$

The head difference causing flow to the skimmer well is given by

$$\Delta h_n = \left(1-\rho_r\right)\left(b_n - b_{nW}\right) \tag{3.57}$$

The corresponding average LNAPL-layer thickness is given by

$$\bar{b}_n = \rho_r\left(b_n - b_{nW}\right)/2 \tag{3.58}$$

With these results the equivalent form of the Dupuit equation becomes

$$Q_n = 2\pi K_{ns}\bar{k}_{nr}\bar{b}_n \frac{\Delta h_n}{\ln\left(R_C/R_W\right)} \tag{3.59}$$

This result may be written

$$Q_n = \frac{\pi\left(1-\rho_r\right)\rho_r T_n\left(b_n\right)\left(b_n - b_{nW}\right)}{\ln\left(R_C/R_W\right)} \tag{3.60}$$

3.3.7 LNAPL Recovery Using Trenches

Equation (3.33) may be used directly to calculate the LNAPL discharge to a trench, where $Q_n = U_n\ L_T$ (L_T is the length of the trench). The water hydraulic gradient includes the natural regional gradient plus any additional gradient associated with groundwater production from the trench. If it is assumed that half of the water discharge comes from each side of the trench, then this additional gradient equals $Q_w/(2K_{ws}L_T b_w)$, where b_w is the effective groundwater capture depth of the trench. The resulting equation for trench LNAPL discharge is

$$Q_n = \frac{T_n\left(b_n\right)L_T}{\rho_r}\left(J_w + \frac{Q_w}{2L_T T_w\left(b_w\right)}\right) \tag{3.61}$$

If the trench bisects an LNAPL lens, then the recovery model may be applied separately to each section of the lens. This is only feasible if water is also produced from the trench to create an

inward gradient on each side. For the section on the downstream side of the trench, the natural water hydraulic gradient J_w should be specified as a negative number.

4 LNAPL CONTINUITY

The purpose of this section is to develop the continuity equations used to predict LNAPL recovery using the models for LNAPL distribution presented in Section 2 and those for LNAPL movement presented in Section 3. A key feature of the proposed model is use of piecewise linear approximations for the LNAPL specific volume and LNAPL transmissibility functions. With these approximations, closed-form analytical solutions to the continuity equations may be obtained for specified regions of LNAPL capture (recovery).

4.1 CONTINUITY EQUATIONS FOR REGIONS OF CAPTURE

In design and analysis of LNAPL recovery systems, the concept of region of capture is inherently related to the continuity principle. The region of capture of a well or trench demarks the area extent from which LNAPL is recovered. In some cases the recovery system geometry may be used to associate a region of capture with individual recovery wells. Consider Figure 4.1 (which is the same as Figure 1.2). The circles shown towards the left side of the figure are centered on 6 possible recovery wells. If each well was producing groundwater, its radius of influence would extend beyond the LNAPL lens. The resulting drawdown cones would overlap, and LNAPL at a particular location would be influenced by all wells with radii of influence that overlap this location. However, the net effect is that the LNAPL would be pulled towards only one well, and this location would be within the region of capture of that well. In a simple analysis the circles shown in Figure 4.1 could demark the region of capture of each well (so called, radius of capture). A more detailed analysis would model the groundwater flow and resulting potentiometric surface, considering the well groundwater production rates and formation hydraulic conductivity field and stratification. For individual wells such as that shown to the right side of Figure 4.1, estimation of the radius of capture is uncertain. This radius could extend out to the radius of influence (for groundwater flow) of the well, but effectively is probably much smaller. Estimation of region of capture remains an important issue for application of the modeling framework.

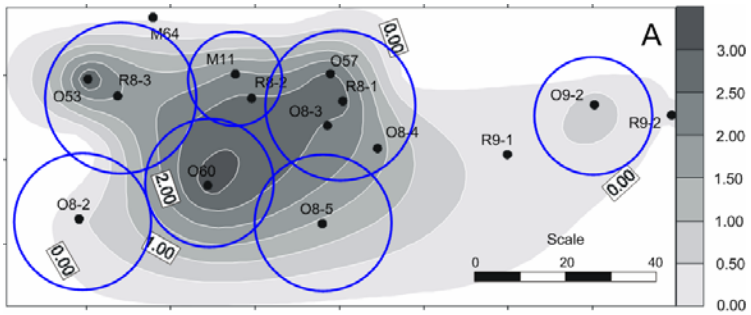

Figure 4.1—Radius of capture based on continuity for the six wells on left, and based on radius of influence for single well on right side of figure

The radius of capture also depends on the technology being used. For a groundwater production well, the radius of influence can easily extend to distances of 500 feet or more. The radius of influence of a vacuum enhances well is limited to about 40 feet or less, while the radius of influence of a skimmer well is probably limited to about 25 feet.

The continuity equation applied to the region of capture zone states that the rate of decrease in LNAPL volume within the region is equal to the LNAPL production rate. Considering only the recoverable volume within a region of capture A_c, the continuity equation may be written

$$-A_c \frac{dR_n}{dt} = Q_n \tag{4.1}$$

In equation (4.1) R_n is the recoverable LNAPL specific volume (equation 2.41) and Q_n is the LNAPL recovery rate. Various rate equations were developed in Section 3. Considering a water-enhanced recovery well for a specific example, equation (3.37) may be combined with equation (4.1) to give

$$-A_c \frac{dR_n(b_n)}{dt} = \frac{T_n(b_n)Q_w}{\rho_r T_w(b_w)} \tag{4.2}$$

During recovery operations, b_n changes with time due to LNAPL production. Thus both R_n and T_n change over time while the other factors are assumed constant. In its general form, equation (4.2) cannot be integrated because both R_n and T_n are nonlinear functions of b_n. However, if one can simplify their representation, then equation (4.2) provides the basis for predicting both recovery volume and rate as a function of time.

4.2 MODEL PARAMETERIZATION AND INTEGRATION

Figure 2.16 suggests that both R_n and T_n are functions of b_n that have simple form and can be approximated using a sequence of linear segments (piecewise linear fit). These are the dashed segments shown in this figure. Between the elevations b_{n1} and b_{n2}, let these functions be fit by linear models of the form

$$R_n(b_n) = \beta(b_n - \chi) \tag{4.3}$$

$$T_n(b_n) = \eta(b_n - \xi) \tag{4.4}$$

It is not difficult to show that for equation (4.3), the unique parameters based on LNAPL thickness values b_{n1} and b_{n2} ($b_{n1} > b_{n2}$) are given by

$$\beta = \frac{R_n(b_{n1}) - R_n(b_{n2})}{b_{n1} - b_{n2}} \tag{4.5}$$

$$\chi = b_{n1} - R_n(b_{n1})/\beta \tag{4.6}$$

A similar result can be found for the parameters η and ξ. With this parameterization equation (4.2) reduces to the form

$$\frac{db_n}{dt} = -\left(\frac{Q_w}{A_c \rho_r T_w(b_w)}\right)\left(\frac{\eta}{\beta}\right)(b_n - \xi) \tag{4.7}$$

Equation (4.7) is a first-order "decay" equation in LNAPL thickness. Similar equations are developed for vacuum-enhanced wells and trenches. The "decay coefficient" is written as the

product of two terms, the first of which is assumed constant, while the second of which will vary from segment to segment of the piecewise linear approximation specified by equations (4.3) to (4.6). Denoting the decay coefficient as a parameter A_j, the solution to equation (4.7) along a segment corresponding from an initial time t_1 to a later time t_2 is

$$b_n(t_2) = \xi_j + (b_n(t_1) - \xi_j) e^{-A_j (t_2 - t_1)} \tag{4.8}$$

In equation (4.8) the form of the parameter A_j will vary with technology and segment of the piecewise linear approximation for R_n and T_n.

For skimmer wells the equations are slightly more complicated. The more general case considers LNAPL recovery from beneath a FGZ (the case without an overlying FGZ has $b_{nW} = 0$). The continuity equation and its integral are

$$\frac{db_n}{dt} = -A_j (b_n - \xi_j)(b_n - b_{nW}) \tag{4.9}$$

$$(t_2 - t_1) = \frac{1}{A_j (\xi_j - b_{nW})} \ln\left(\frac{(b_n(t_1) - \xi_j)(b_n(t_2) - b_{nW})}{(b_n(t_2) - \xi_j)(b_n(t_1) - b_{nW})} \right) \tag{4.10}$$

In model implementation, the second segment of the piecewise linear fit is selected so that $\xi_2 = b_{nW} = b_{n1}$. In this case the differential equation becomes

$$\frac{db_n}{dt} = -A_j (b_n - b_{nW})^2 \tag{4.11}$$

The integral gives

$$A_j (t_2 - t_1) = \frac{1}{b_n(t_2) - b_{nW}} - \frac{1}{b_n(t_1) - b_{nW}} \tag{4.12}$$

These are the basic solutions to the continuity equation for the model formulation. They are summarized in somewhat more detail in Table 4.1. Implementation of the model for LNAPL recovery using pumping wells, vacuum-enhanced wells, skimmer wells, and trenches is discussed in Volume 2.

Table 4.1. LNAPL Recovery System Performance Equations

	Water Pumping/Vacuum Enhanced/Trench	Skimmer
Continuity	$\frac{db_n}{dt} = -A_{kj}\left(b_n - \xi_j\right)$	$\frac{db_n}{dt} = -A_{kj}\left(b_n - \xi_j\right)\left(b_n - b_{nW}\right)$
Performance coefficient	$A_{wj} = \frac{Q_w}{\pi R_c{}^2 \rho_r T_{w-bw}}\left(\frac{\eta_j}{\beta_j}\right)$ $A_{aj} = \frac{\mu_{ar} Q_a}{\pi R_c{}^2 \rho_r \bar{k}_{ra} T_{w-ba}}\left(\frac{\eta_j}{\beta_j}\right)$ $A_{tj} = \frac{1}{\rho_r W_T}\left(I_w + \frac{Q_w}{2L_T T_w}\right)\left(\frac{\eta_j}{\beta_j}\right)$	$A_{sj} = \frac{\left(1-\rho_r\right)}{R_c{}^2 \ln\left(R_c/R_w\right)}\left(\frac{\eta_j}{\beta_j}\right) \quad [b_{nW} = 0]$ $A_{sj} = \frac{\left(1-\rho_r\right)\rho_r}{R_c{}^2 \ln\left(R_c/R_w\right)}\left(\frac{\eta_j}{\beta_j}\right) \quad [b_{nW} \neq 0]$ (LNAPL Beneath FGZ)
Performance equation	$b_n\left(t_2\right) = \xi_j + \left(b_n\left(t_1\right) - \xi_j\right)\exp\left(-A_{kj}\left(t_2 - t_1\right)\right)$	$A_{sj}\left(t_2 - t_1\right) = \frac{1}{\xi_j - b_{nW}} \ln\left(\frac{\left(b_n\left(t_1\right) - \xi_j\right)\left(b_n\left(t_2\right) - b_{nW}\right)}{\left(b_n\left(t_2\right) - \xi_j\right)\left(b_n\left(t_1\right) - b_{nW}\right)}\right)$
Performance equation ($\xi_j = b_{nW}$) [including = 0]		$A_{sj}\left(t_2 - t_1\right) = \frac{1}{b_n\left(t_2\right) - b_{nW}} - \frac{1}{b_n\left(t_1\right) - b_{nW}}$

References

Adamson, A.W. (1982). *Physical Chemistry of Surfaces*, 4th Ed., Wiley-Interscience, New York.

Adamski, M., Kremesec, V., Kolhatkar, R., Pearson, C., and Rowan, B. (2005). "LNAPL in fine-grained soils: conceptualization of saturation, distribution, recovery, and their modeling." *Ground Water Monitoring & Remediation, 25*(1), 100-112.

Adamski, M., Kremesec V., and Charbeneau, R.J. (2003). "Residual Saturation: What is it? How is it measured? How should be use it?" Petroleum Hydrocarbons Conference, National Ground Water Association, Costa Mesa, CA, August 19-20. Printed in 2005 Proceedings pp 243-250.

API Interactive LNAPL Guide, Version 2 (2004). American Petroleum Institute, Washington D.C. (http://api-ep.api.org/environment/index.cfm)

Bear, J. (1972). *Dynamics of fluids in porous media*. American Elsevier Pub. Co., New York.

Brooks, R.H. and Corey, A.T. (1964). "Hydraulic properties of porous media." *Hydrol. Pap. 3*, Colo. State Univ., Fort Collins.

Burdine, N.T. (1953). "Relative permeability calculations from pore-size data." *Trans. A.I.M.E. 198*, 71-77.

Charbeneau, R.J., Weaver, J.W. and Lien, B.K. (1995). *The Hydrocarbon Spill Screening Model (HSSM), Volume 2: Theoretical background and source codes*. EPA/600/R-94/039b, Robert S. Kerr Environmental Research Laboratory, U.S. Environmental Protection Agency, Ada, Oklahoma.

Charbeneau, R.J., Johns, R.T., Lake, L.W. and McAdams III, M.J. (1999). *Free-product recovery of petroleum hydrocarbon liquids*. API Publication Number 4682, American Petroleum Institute, Washington D.C.

Charbeneau, R.J. (2000). *Groundwater hydraulics and pollutant transport*. Prentice Hall, Englewood Cliffs.

Charbeneau, R.J. (2003). *Models for design of free-product recovery systems for petroleum hydrocarbon liquids*. API Publication Number 4729, American Petroleum Institute, Washington D.C.

Corey, A.T. (1986). *Mechanics of immiscible fluids in porous media*, 2nd Ed., Water Resources Publications, Littleton, Co.

Drake, L.C. and Ritter, H.L. (1945). "Pore size distribution in porous material." *Ind. Eng. Chem. Anal., 17*, 782-787.

Dullien, F.A.L. (1992). *Porous media: fluid transport and pore structure*, 2nd Ed., Academic Press, San Diego.

Farr, A. M., R. J. Houghtalen, and McWhorter, D.B. (1990). "Volume estimation of light nonaqueous phase liquids in porous media." *Ground Water, 28*(1), 48-56.

Hillel, D. (1980). *Fundamentals of Soil Physics*. Academic Press, San Diego.

Hubbert, M.K. (1954). "Entrapment of petroleum under hydrodynamic conditions." *Bull. Am. Assoc. Petroleum Geologists, 37*, 1954-2026.

Huntley, D. and Beckett, G.D. (2002). *Evaluating hydrocarbon removal from source zones and its effect on dissolved plume longevity and magnitude*. API Publication Number 4715, American Petroleum Institute, Washington D.C.

Johns, R.T., Lake, L.W., Obigbesan, A.B., Bermudez, L., Hassan, M.R. and Charbeneau, R.J. (2003). "Analytical solutions for free-product recovery using skimmer and dual-pump wells." *Ground Water Monitoring and Remediation, 23*(1), 97-106.

Johnston, C.D. and Adamski, M. (2005). "Relationship between initial and residual LNAPL saturation for different soil types." Petroleum Hydrocarbons Conference, National Ground Water Association, Costa Mesa, CA, August 17-19, pp 29-42.

Kueper, B.H., Redman, D., Starr, R.C., Reitsma, S., and Mah, M. (1993). "A field experiment to study behavior of tetrachloroethylene below the water table: spatial distribution of residual and pooled DNAPL," *Ground Water*, 31, 756-766.

Leferbvre, R. (2000). Personnel communication.

Lenhard, R. J. and Parker, J.C. (1990). "Estimation of free hydrocarbon volume from fluid levels in monitoring wells." *Ground Water, 28*(1), 57-67.

Leverett, M.C. (1941). "Capillary behavior in porous media." *Trans. A.I.M.E. 142*, 341-358.

Muskat, M. (1946). *The flow of homogeneous fluids through porous media*. Edwards, Ann Arbor.

Mercer, J.W. and Cohen, R.M. (1990). "A review of immiscible fluids in the subsurface: properties, models, characterization, and remediation," *J. Contaminant Hydrology*, *6*, 107-163.

Steffy, D.A., Barry, D.A., and Johnston, C.D. (1997). "Influence of antecedent moisture content on residual LNAPL saturation," *J. Soil Contamination, 6*(2), 113-147.

Mualem, Y. (1976). "A new model for predicting the hydraulic conductivity of unsaturated porous media," *Water Resourc. Res., 12*, 513-522.

Parker, J.C., Lenhard, R.J., and Kuppusamy, T. (1987). “A parametric model for constitutive properties governing multiphase flow in porous media.” *Water Resour. Res., 23,* 618-624.

Van Genuchten, M.Th. (1980). “A closed-form equation for predicting the hydraulic conductivity of unsaturated soil.” *Soil Sci. Soc. Am. J., 44,* 892-898.

Van Genuchten, M.Th., Leij, F.J., and Yates, S.R. (1991). *The RETC code for quantifying the hydraulic functions of unsaturated soils*. EPA/600/2-91/065, Robert S. Kerr Environmental Research Laboratory, U.S. Environmental Protection Agency, Ada, Oklahoma.

Waddill, D.W. and Parker, J.C. (1997). “Simulated recovery of light, nonaqueous phase liquid from unconfined heterogeneous aquifers,” *Ground Water, 35*(6), 938-947.

Weaver, J.W., Charbeneau, R.J., Tauxe, J.D., Lien, B.K., and Provost, J.B. (1994). *The hydrocarbon spill screening model (HSSM), Volume 1: User’s Guide*, EPA/600/R-94/039a, Robert S. Kerr Environmental Research Laboratory, U.S. Environmental Protection Agency, Ada, Oklahoma.

Zhou, D. and Blunt, M. (1997). “Effect of spreading coefficient on the distribution of light non-aqueous phase liquid in the subsurface.” *J. Contaminant Hydrology, 25*, 1-19.

Additional copies are available through IHS
Phone Orders: 1-800-854-7179 (Toll-free in the U.S. and Canada)
303-397-7956 (Local and International)
Fax Orders: 303-397-2740
Online Orders: global.ihs.com

Information about API Publications, Programs and Services
is available on the web at **www.api.org**

1220 L Street, NW
Washington, DC 20005-4070
USA

202.682.8000

Product No. I47600